Potential applications of nanotechnology in bioenergy

Jason Kramb

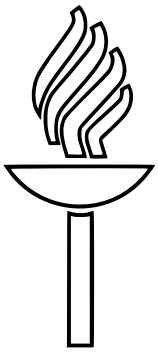

Master's thesis
Master's Degree Program in Renewable Energy
Department of Physics, University of Jyväskylä
Supervisors: Jukka Konttinen, Jussi Maunuksela
July 1, 2011

Abstract

Nanotechnology has an increasingly large impact on a wide range of industries, but its current use in the production of electricity and heat from biomass is limited. This thesis examined the potential impact of nanotechnology on bioenergy production through a literature review and interviews with industry members. Current technologies and methods in use were reviewed, with a focus on fuel handling and combustion systems. Areas in which problems existed were identified and nanotechnologies with properties relevant to those problems examined. The major nanotechnology areas which were reviewed are nanostructured coatings (wear resistant, corrosion resistant, low friction and anti-icing), nanomembranes for gas separation, nanostructured catalysts for emission reductions, thermoelectrics and thermophotovoltaics. Basic economic analyses were also performed to determine conditions for economic viability of the nanotechnology solutions. The thesis concludes that while there are many areas which have promising technologies in development, there are no clear nanotechnology solutions which can be implemented cost effectively at the current time. Recommendations for future work are also made.

Preface

I would like to thank the supervisors of this work: Dan Asplund (Benet Oy), Jukka Konttinen (University of Jyväskylä) and Jussi Maunuksela (University of Jyväskylä). I would also like to thank Juha Huotari (MW Power), Kauko Isomöttönen (Vapo Oy), Timo Järvinen (VTT) and Elja Kallberg (University of Jyväskylä) for providing valuable assistance. Funding for this project was provided by Benet Oy with support from The Jyväskylä Region Centre of Expertise Programme.

Contents

List of Figures

Chapter 1

Introduction

Nanoscience and the technologies that result from it are to have huge impacts on a wide range of industries. Dozens of academic publications can be found which discuss a potential nanoscience backed scientific or industrial revolution. The impacts, both realized and potential, of nanoscience and nanotechnology on the medical field, biotechnology, food production, electronics and numerous other areas of concern have been studied and reported. The potential impacts of nanotechnology on energy production from biomass will be examined in this paper. A focus will be given on short to medium term timeframes and to energy production in central Finland using primarily forest based biomass and peat.

1.1 Forest biomass for energy production

Combustion of biomass has been a primary source of energy for humans throughout much of history. In the twentieth century biomass was largely replaced by fossil fuels in the developed world but it continued to be an important fuel source. In the late twentieth and early twenty-first centuries a growing concern with potential negative consequences associated with the use of non-renewable fossil fuels has caused a resurgence of interest in biomass in many countries.

Unlike in most developed countries, biomass has remained one of the primary fuel sources for heat and electricity production in Finland. In 2009 wood based fuels and peat accounted for approximately a quarter of the total energy consumption of the country, at 20 and 5,4 percent respectively [1]. This corresponds to about 339 000 terajoules of energy. For comparison the energy consumption per capita in the United States was 1,3 times greater than that of Finland, however the per capita energy consumption from biomass fuels was 4,7 times greater in Finland than in the U.S. [2].

1.2 Nanoscience and nanotechnology

Nanoscience and nanotechnology involve the manipulation of matter on a nanoscale, nanoscale refering to a size range of roughly one to 100 nanometers. This definition is

not uniformly applied however, and the use of the label 'nano' has remained somewhat subjective. More generally it can be used to describe any science or technology related to the manipulation of matter on the atomic and molecular scale.

Research in nanoscience has increased rapidly over the last twenty years. In the eight years between 1997 and 2005 governmental funding for nanoscience research increase 9-fold to $4,1 billion [3]. The number of scientific publications and journals covering nanoscience topics has increased as well during this time. By 1998 there had been fifteen journals on nanotechnology launched, while by 2010 that number had increased to 165 [4]. One study [5] identified more than 50 000 academic articles published on nanoscience topics in 2006 alone, and similar amounts being published in the following years.

1.3 Outline of the thesis

Chapter two consists of a literature review which covers the current technologies and processes used in the bioenergy industry, problems associated with those technologies and process, and potential solutions to those problems using nanotechnology. Much of the initial information on the problems in the current bioenergy industry came from people and companies involved in the industry but has been supported with published literature. Chapter three provides an economic analysis of a sample of the nanotechnology solutions discussed in Chapter two. Chapter four gives a discussion of the findings.

Chapter 2

Literature Review

The production of electricity and high temperature steam from biomass is a complicated process. Some of the complications involved are due to the nature of the energy production industry and similar problems can be found when using other fuels, such as coal or natural gas. Biomass also has its own unique problems, and due to the local nature of most biomass fuels, many of those problems vary from region to region as the composition of the biomass fuels change. This literature review focuses on select problems associated with the combustion of biomass in central Finland and nanotechnology solutions to those problems. The biomass fuels of primary concern are forest residue, other wood based fuels and peat.

2.1 Current technologies and methods

Current methods in use by the energy and forestry industries for the purposes of transportation and handling of biomass fuel, fuel combustion and waste heat recovery are discussed in sections 2.1.1 through 2.1.4. While these topics all depend strongly on the details of the particular power plant an attempt has been made to present a generalized view.

2.1.1 Transport

Transport by lorry is, in general, the most common method used to deliver biomass fuel to power plants. A medium sized lorry can transport 120 m^3 of biomass. Small biomass power plants may require as few as five deliveries of this size per day, while a larger power plant may require 90 or more. The type of lorry used is largely determined by the type of biomass being transported, as each type can require a different container. Unloading the contents of the container upon reaching the power plant is most often done through tipping the container either backwards or to the side, depending on the receiving facilities of the plant.

Trains are used to transport biomass over long distances. Most biomass used in energy production is transported between fifty and one hundred kilometers, making train transport for biomass often impractical. Biomass power plants may also be able to co-fire using coal. Power plants with this capability may have train receiving facilities for delivery of coal.

2.1.2 Handling

Depending on the power plant the biomass fuel will have different particle size requirements; chippers and hammermills are used to reduce the size of the biomass to the appropriate dimensions. Chippers are generally used to create particles of size 5-50 mm, while hammer mills can create particles of size less than 5 mm. Chippers use a sharp knife, or knives, to cut away part of the wood. Hammermills use hammers rather than knives to reduce the size of the biomass. The hammers are connected to a rotating shaft which is enclosed in a container, often a steel drum. A screen on the container allows material of the appropriate size to pass through. The rotor is spun at high speed and material is fed into the container. The hammers impact the material and it is shredded until the size is small enough to pass through the screen. Figure 2.1 shows an industrial scale hammermill grinding wood waste and Figure 2.2 shows a schematic of the operating principle of the hammermill.

Figure 2.1: Dynamic 5240 horizontal grinder and hammermill [6].

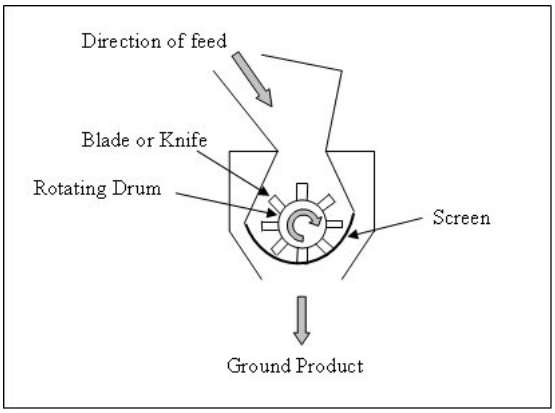

Figure 2.2: Schematic diagram of hammermill [7].

For a power plant to produce a constant level of power output the fuel feed rate to the boiler must be relatively constant. The rate fuel is delivered to the power plant is not constant however, as it varies with the arrival of vehicles used for the transport of the fuel. This means that intermediate storage facilities are needed at the power plant to hold the fuel when delivered until it is needed by the boiler. The number and size of these intermediate storage facilities will vary based on the details of the power plant, such as the method of transportation of the fuel, the rate of fuel delivery to the plant,

the rate of fuel consumption of the boiler, and the type of fuel used. The storage method itself can also vary depending on the fuel properties, environmental conditions and fuel consumption rate of the plant. Silos, bin storage and open yards are all used for the storage of biomass. The longest term storage facility is most often the largest and a small storage silo is sometimes used just before the fuel is fed into the boiler. For a small scale power plant this boiler silo can be five to ten m^3 in volume, and is constantly being refilled as it contains only enough fuel for a few minutes of power production. The purpose of this silo is less for storage than for providing a constant and uninterrupted flow of fuel to the boiler [8] [9]. Figure 2.3 shows a schematic drawing of a simplified fuel handling system for a biomass plant.

Movement of material between storage facilities can be done using a wide variety of equipment. Conveyors are a common method used for this purpose. There are a variety of conveyor systems which can be used for different situations. Drag chain conveyors operate by a continuous chain which runs the length of the conveyor and is connected to a drive unit. The material to be transported can then be pulled or pushed using the chain. In a form that is commonly used with biomass metal bars are connected to two chains which run parallel to each other at either side of the conveyor trough. The metal bars then push the material along the conveyor path. Drag chain conveyors are well suited for use with abrasive materials, tall materials, and when transport up an incline is needed. Drag chain conveyors are commonly used for bulk biomass for these reasons and due to the potentially non-uniform size of the fuel [10]. Hardened steel is often used in the high wear locations of the handling system, such as the bottom of the conveyors or the gliding rails. Raex AR 500 is a hardened wear-resistant steel used for this purpose in some Metso-Wärtsilä designed biomass power plants. It is designed for use in wear pads and has a hardness of over three times that of S355 structural steel.

Belt conveyors are also used when possible. Belt conveyors can generally be run at a faster speed, moving material more quickly, and use less power than drag chain conveyors but can be used with a more limited selection of fuel [8]. Peat can be transported on belt conveyors and is done so at the Rauhalahti power plant [12].

Cranes are also used in some situations to move fuel between storage facilities. The most common use for them is to move material out of a long term storage container [8]. A grab crane system is used in Metso-Wärtsilä BioPower plants when extra storage capacity for longer intervals between fuel deliveries is required [13], and is shown in Figure 2.4. In this case the storage volume is usually between 2500 and 3000 m^3, which for a medium sized power plant can last two or three days.

2.1.3 Energy conversion/fuel combustion

Power plants using exclusively biomass are generally on the size of a few hundred megawatts or less. This is most often due to the lower net caloric values of biomass

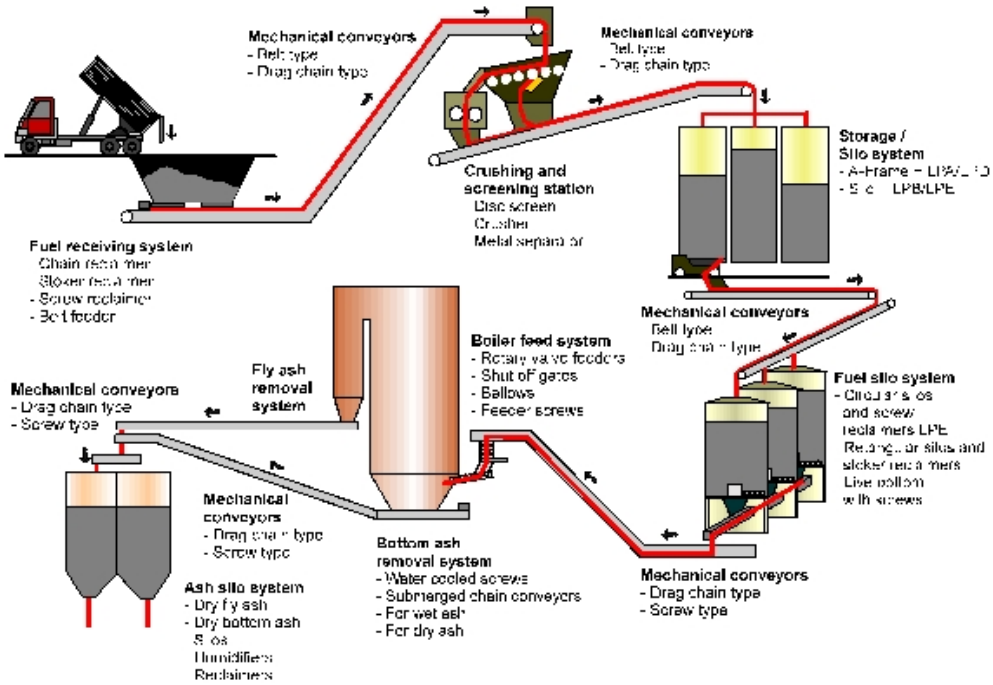

Figure 2.3: Schematic diagram of biomass fuel handling system [11].

compared with fossil fuels. This typically results in larger volumes of biomass fuel being needed to produce an equivalent power output when compared with fossil fuel power plants, and so the size of a biomass power plant can be limited by how much fuel can be practically delivered to the plant and at what rate. The larger the boiler size the less likely local biomass will be able to meet the plant's fuel needs as well, reducing some of the environmental benefits to using biomass [14]. While there have been design challenges in scaling up the size of biomass boilers, the average size has tended to increase over the last two decades [15]. Currently, large sized biomass power plants are of the size range 200 MW electrical (MW_e) [16] or 500 MW combined heat and electricity [17].

2.1.3.1 Boiler types

There is a wide variety of technology used for the combustion of biomass. In Finland grate furnaces and fluidized bed furnaces are the most commonly used type of furnace. For small power plants grate furnaces are more common, but as the size of the power plant increases fluidized bed furnaces become more attractive. Schematic drawings of grate, bubbling bed and circulating fluidized bed boilers are shown in Figure 2.5.

Grate furnaces are those in which the combustion of the fuel takes place on a grate surface, located towards the bottom of the furnace. The primary air for the combustion of the fuel is usually added from below the grate. Secondary air is added at a higher level for burning of the combustible gases. An important principle in the operation of grate boilers is that the fuel must be spread evenly over the grate for best performance. There are

Figure 2.4: Grab crane system used in Mesto-Wärtsilä BioPower plants [13].

various types of grate fired boilers, each with advantages and disadvantages. In a sloping grate boiler the grate itself does not move, it is simply sloped downward and the fuel burns as it slides down the grate. Travelling-grate and vibrating-grate boilers both involve moving grates which distribute the fuel evenly [18]. Figure 2.6 shows the Biograte boiler produced by Metso-Wärtsilä and used in their small scale BioPower biomass combustion plants. Biograte boilers use a rotating grate and can produce up to 5,6 MW_e if maximum electrical output is desired or a combination of 3,8 MW_e and 13,5 MW_{th} if maximum combined electrical and thermal output is desired.

In a fluidized bed furnace the fuel does not rest on a grate during combustion. The fuel is suspended by the combustion air which is added below the fuel and rises with enough force to lift the fuel. The bed is composed of sand or other solid material which is suspended with the fuel. The two most common categories of fluidized bed furnaces are bubbling and circulating fluidized beds. The primary difference between these groups is the velocity of the combustion air which is added from below the fuel and particle size of the bed material. In a circulating fluidized bed furnace the velocity is great enough to lift the bed material with the flue gases. In a bubbling bed furnace the bed material remains with the fuel and is not lifted with the flue gases.

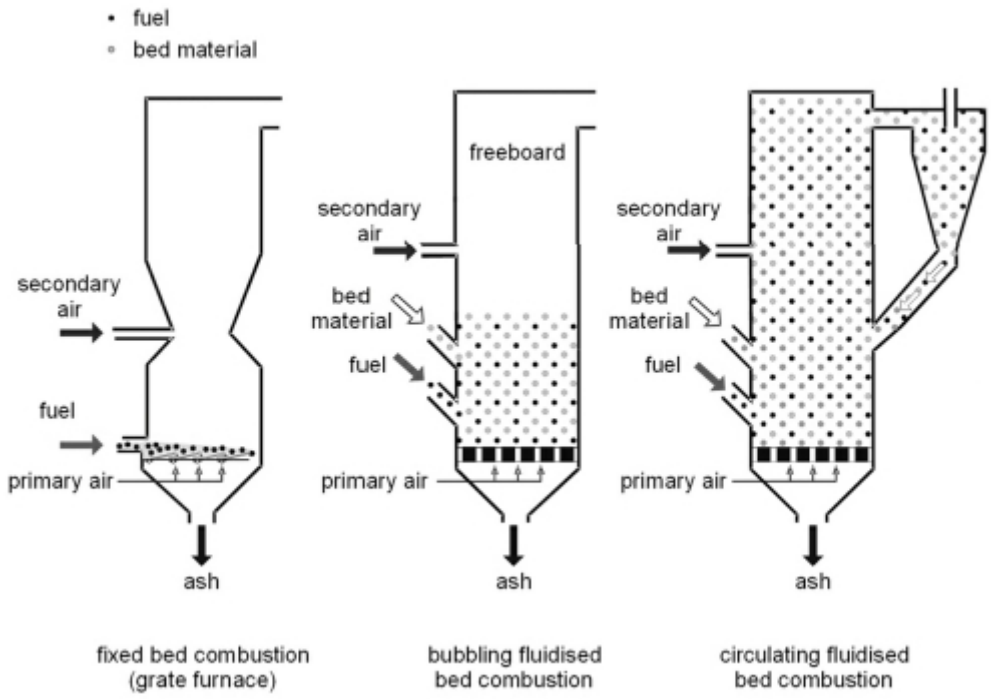

Figure 2.5: Schematic drawings of the three most common types of biomass furnaces in Finland: grate, bubbling fluidized bed, and circulating fluidized bed [8].

2.1.3.2 Ash deposits, corrosion and erosion

Ash deposits, corrosion and erosion inside the boiler are all problems which exist with almost any fuel, and biomass is no exception. The primary cause of all three of these are inorganic materials in the biomass, namely alkali and alkaline earth metals and chlorine. For biomass the alkali of primary concern is potassium. Baxter et al. [19] reported that for a variety of biomass fuels, focusing largely on straws and shells, potassium concentrations ranged from less than 0,1% to over 3% while chlorine ranged from 0,05% to 0,55%. Of the fuels examined Swedish wood was shown to have comparatively a much lower potassium and chlorine concentration. Chlorine concentration was 0,01% and as of the dry weight, while potassium oxide (K_2O) was 9,46% of the ash content, making it 0,0001% of the total fuel by weight [20]. Hiltunen et al. [21] reported that the average K_2O percentage by weight of ash from forest residue was 9,2%, while for peat it was 1.4%. In general wood fuels are considered to have relatively good characteristics with regard to these problematic substances.

The inorganic materials may be vaporized during combustion of the biomass fuel. The amount and type of inorganic materials vaporized during combustion is based on many factors, including the temperature at which the combustion occurs, the concentrations of the inorganics in the fuels, and the amount of the combustion gases available. Chlorine in biomass fuels has been shown to promote the vaporization of alkali in the fuel during combustion. The concentration of chlorine was shown to often be more important than

Figure 2.6: Biograte boiler used in Mesto-Wärtsilä BioPower plants [13].

the alkali concentration in the amount of alkali vaporization [19]. Figure 2.7 shows a schematic drawing of possible deposit forming locations and generalized pathways which potassium, sulfur and chlorine might take in a biomass boiler.

Deposit formation is often grouped into two categories: slag and fouling. Slag deposits refer to those which form on surfaces which receive direct radiation from the flame, while fouling deposits are on convective surfaces such as the heat exchangers. Deposits can occur at both high and low temperatures and their formation in the boiler is generally attributed to four mechanisms: inertial impaction, thermophoretic deposition, condensation, and chemical reaction [19] [22]. Deposit formation anywhere in the boiler is undesired and can lead to a wide range of negative effects. Deposits on water walls, superheaters and heat exchangers can reduce heat absorption through these surfaces. Ash deposits can increase corrosion rates on many types of surfaces. Shedding of large ash deposits on high surfaces can damage lower surfaces upon impact. There can be many other negative consequences of deposit formation based on the boiler, deposit composition and the location of the deposit [8].

The atmosphere of a boiler can lead to corrosion of metal surfaces. This corrosion can be accelerated by ash deposits. Corrosion can, and does, occur on all metal surfaces inside the boiler to some extent and for biomass boilers the principal concern is high temperature corrosion inside the superheater [8]. In general the corrosion of greatest concern in biomass combustion can be described as either due to oxidation or due to chlorine. The high temperature corrosion process has been described in numerous publications, including by Latreche [24], Worch [25] and others.

In oxidizing environments some materials develop oxide films on their surface due to corrosion. In some cases these films, called scales, act as a barrier between the material

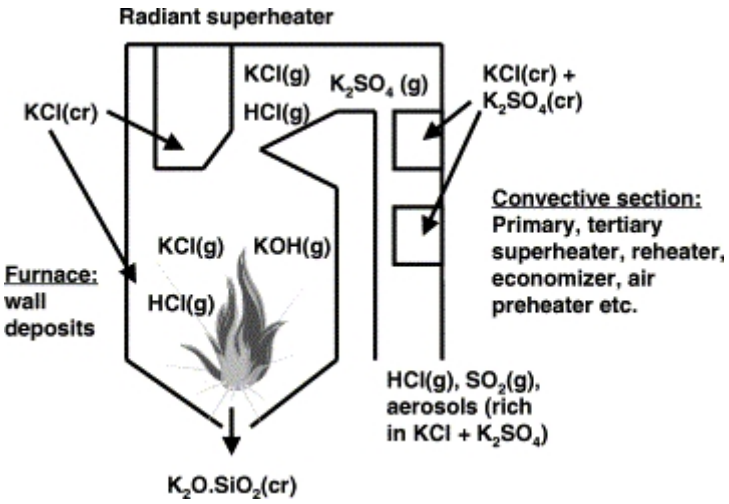

Figure 2.7: Generalized pathways for potassium, sulfur and chlorine in a boiler [23].

and the environment. The metal, or the environment, must diffuse through the scale for the corrosion to continue. The formation and retention of these scales is important to the functioning of most anti-corrosion materials in an oxidizing environment [26]. It is common for boiler applications for these scales to consist of Al_2O_3 or Cr_2O_3 [27]. The reaction of a metal and oxygen gas to form these scales can we written simply as shown in equation 2.1 [24],

$$aM(s) + \frac{b}{2}O_2(g) = M_aO_b(s). \tag{2.1}$$

The main stages of this process are shown in Figure 2.8.

However, due to the presence of chlorine in biomass fuels these oxide scales are not entirely protective in biomass boilers. Chlorine is able to penetrate the scales and react with the metal at the scale-metal border [23] [28]. Similar to equation 2.1, the reaction of metal and chlorine gas to form a metal chloride can be written as shown in equation 2.2 [24],

$$xM(s) + \frac{y}{2}Cl_2(g) = M_xCl_y(s) = M_xCl_y(g). \tag{2.2}$$

Bender et al. [29] describes the circular process in which gaseous chlorine attacks metals in high temperature oxygen containing environments. This is shown in Figure 2.9. Despite this, Nielsen reports that some coatings are still effective for corrosion protection for short periods of time in chlorine containing atmospheres [28] and under chlorine containing salt deposits [30].

As high temperatures increase corrosion rates, one of the primary means to prevent corrosion has been to lower temperatures inside superheater tubes. These temperatures can range from below 450 °C [23] to 490 °C, while coal boilers often have superheater steam temperatures above 540 °C [31]. This solution is undesirable in many cases however, as

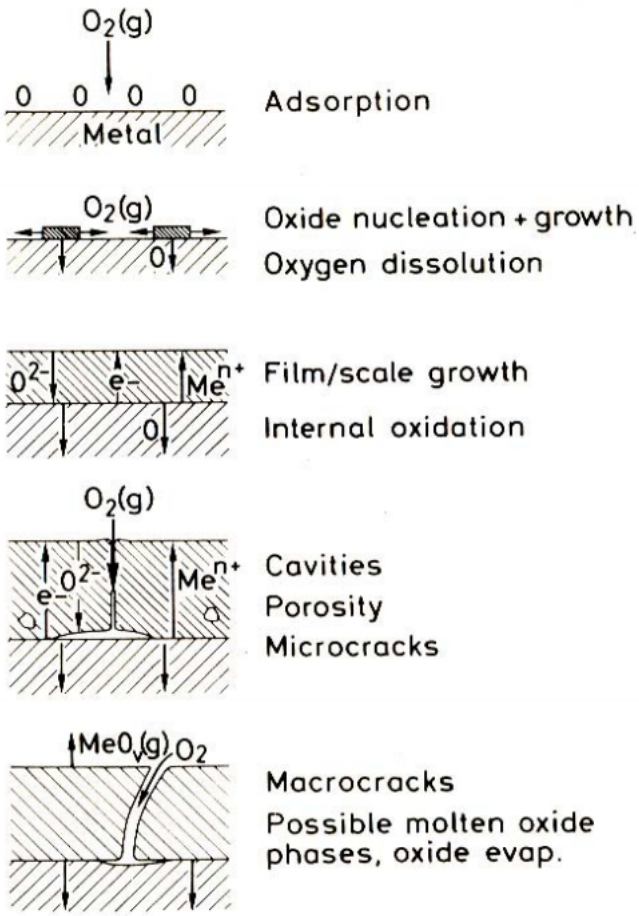

Figure 2.8: Schematic diagram of the main stages in the formation of an oxide scale [25].

the electrical generation efficiency can be increased by increasing the steam temperature. Fuel additives can also be used to reduce the concentration of certain substances in the ash, and this is seen as a primary way to reduce corrosion. Kaolin, a clay mineral, has been shown to be an effective additive for reducing chlorine deposition in fluidized bed boilers at temperatures typical of superheaters [32]. ChlorOut, produced by Vattenfall, is another fuel additive has also been shown to reduce chlorine concentrations and corrosion.

Biomass in general, and especially wood fuels, have low ash contents and are therefore seen as less prone to causing erosion damage in the boiler. However, erosion can still occur in biomass boilers and cause problems during operation. While erosion and corrosion can be unrelated, Wang [33] reported that corrosion accelerated erosion was the major erosion mechanism of concern in biomass boilers. Erosion can also be of increased concern in fluidized bed boilers using biomass, due to high solid velocities inside the boiler [34]. Wang has also reported that the material wastage of thermally sprayed coatings in biomass boilers is more heavily dependent on the coating microstructure and composition than on the hardness. This again reflects the fact that the most common erosion is accelerated by corrosion rather than caused entirely by impact of particles on the metal surfaces.

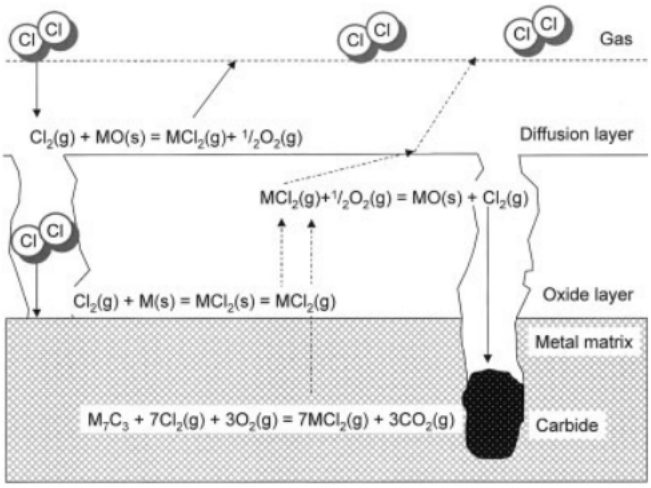

Figure 2.9: Schematic of possible methods of chlorine attack in high temperature oxygen containing environments [29].

Thermal spray coatings are used to protect boiler components from corrosion. Thermal sprays refer to a coating in which a material is melted and then sprayed onto a surface. There are numerous different variations of the thermal spray technique and the coatings can be up to a few millimeters thick. Nickle-chormium and iron-chromium alloys are examples of materials which can be used for this purpose [35][36]. Tuurna et al. [37] showed that using such materials with coating thickness of between 150 and 350 micrometers provides "excellent" corrosion resistance to atmospheres with chlorine, such as those produced by the combustion of biofuel.

2.1.3.3 Emissions

Emissions from biomass combustion could also be improved. While harmful emissions are generally lower than fossil fuel burning power plants, biomass combustion does still produce nitrogen oxides, sulphur oxides and, of course, carbon dioxide. Nitrogen oxides are present mainly in the form of NO, while sulphur oxides are mainly SO_2. In biomass burning power plants, the emission of these chemicals are reduced primarily by preventing the formation of the chemicals inside the boiler, through the use of so called primary emission reduction measures. These measures can include changing properties of the fuel, such as fuel composition and particle size, and improving the design of the combustion chamber. Catalytic converters are also used to reduce emissions from biomass combustion, though the use of the converters is generally limited to small scale combustion such as wood burning stoves. They are also primarily used for the removal of carbon monoxide from the flue gas [38]. Selective catalytic reduction (SCR) is another catalytic process which can be used in biomass combustion to improve emissions, this time by reducing NO_x from the flue gas. SCR is used primarily on coal fired power plants but can also

be used with biomass fueled and co-fired plants, though significant problems occur which are discussed in section 2.3.3. Secondary emission reduction measures are those which remove emissions from the flue gas after it has left the boiler. These measures can include equipment such as electrostatic filters and wet scrubbers. [8]

2.1.4 Waste heat recovery

Biomass can also be particularly well suited for a combined heat and power (CHP) plant. The forest industry in Finland makes extensive use of this and CHP plants are often located near large pulp and paper mills, using the by products of the plant to provide the energy needed by the plant. The forest industry provided itself with 42% of the 25,5 TWh it consumed in 2001 [39].

Combined heat and power production is also used for district heating. Over 25 percent of the district heating CHP in Finland uses biomass fuel. CHP plants can have particularly high overall energy efficiencies, as high as 94% in some cases [40]. For small, decentralized CHP plants an overall energy efficiency of 80% is more reasonable [8].

There are other methods available to improve the efficiency of biomass power plants. Flue gas condensation can provide energy recovery of up to 20% of the net calorific value of the input fuel [8]. Feedwater preheating and steam reheating can also increase energy efficiencies. These methods are evaluated based on the details of each individual plant to determine its effectiveness.

2.2 Current nanotechnology uses in bioenergy production

While nanotechnology products are currently being produced and utilised in a number of fields nanotechnology has yet to see widespread use in the bioenergy industry. This is due to a number of limiting factors including technical and economic issues, which are present in the nanotechnologies and in the bioenergy sector. While no examples of nanotechnology could be found currently in use in the Finnish bioenergy industry, there are many examples of new materials being used to improve performance. One example of this is shipping containers developed by the company Fibrocom. These containers are made from a patented 'Channel composite'® material which provides high strength and damage resistance. These containers are lighters than convention counterparts and allow the trucks to transport more material than would otherwise be possible. They are currently being used by Vapo Oy for the transportation of peat. [41][42]

2.3 Needs for improvement

Like any energy production system, the process of energy production from biomass could be improved in numerous ways. Sections 2.3.1 through 2.3.4 discuss a few specific examples of such areas. These areas for improvement were proposed largely by people working in bioenergy industry and have therefore come from experience working with the modern equipment and methods described in section 2.1.

2.3.1 Transport

Biomass, and particularly peat, used in electricity and heat generation can have high moisture content when compared with fossil fuels such as coal. Moisture content between forty and fifty-five percent is common for peat in Finland. This high moisture content can lead to a number of complications, including freezing of the fuel to the truck surfaces during transportation. This most often occurs during the transport of peat in very low temperatures when the fuel is in direct contact with metal surfaces such as steel. Heating systems and de-icing spray can be used to unfreeze the peat from the truck, but in some situations the peat must be removed manually.

As with the transportation of any fuel or other product the weight of the transportation vehicle and shipping container can also be a problem. If the weight of the vehicle and container could be decreased, the amount of biomass which could be transported per truck could increase. This is of particular interest to biomass as the fuel density is lower than competing fuels such as coal, causing increased transportation costs. Also, as mentioned in section 2.1.3, the rate of biomass delivery to a power plant can be a limiting factor in the size of a plant. Increased truck carrying capacity could potentially allow for larger fuel delivery rates and increased power plant size.

2.3.2 Handling

The primary problem of concern during the handling of the biomass at the power plant is the behavior of the biomass in the boiler silo. This is the final storage container before the fuel enters into the boiler. In the BioPower power plant designs by Metso-Wärtsilä the boiler silo is adjacent to the boiler itself. During the winter the temperature difference between the storage silo and boiler silo can be 40 °C, as the storage silos are at the outside ambient temperature and the boiler silos are often around 20 or 30 °C.

When milled peat enters the boiler silo it has a tendency to stick to the walls of the silo. More peat particles adhere to the original layer and this can continue until a significant portion of the boiler silo is obstructed. This can lead to interruptions in the fuel supply to the boiler as fuel cannot be added to the boiler silo fast enough.

A related problem can occur when the biomass adheres to the wall of the boiler silo at a lower level. This can cause biomass to accumulate above the stuck layer, but there

will be no fuel below it. If the sensors are placed above the stuck biomass they will read that fuel is present, when in fact this is not true. This can again lead to interruptions in fuel supply to the boiler.

Mechanical wear is a constant problem in bioenergy production, as it is in many other industries. Wear occurs in all moving components of the fuel handling systems to some degree but occurs most severely in certain areas. The two areas which were examined are hammermills and conveyor systems.

Hammermills see extreme wear on the hammers used to crush biomass fuel. Under normal operating conditions these hammers can require replacement monthly. When tree stumps are fed into the machine they contain a larger amount of dirt, sand and stones and can reduce the operation life of the hammers even further. Many hammers are made from, or have a coating of, tungsten carbide (WC) to reduce wear and increase their life. Even with such a coating replacement time is still more often measured in weeks rather than months. Figure 2.10 shows a hammer used in a hammermill on which a tungsten carbide weld coating has been applied. The hammer is swung from the hole on the left side and the right side of the hammer has a tungsten carbide spray on the leading edges. Both the top and bottom edge are coated with WC so that the hammer can be rotated in order to extend its operational life. When the bottom right side is used as the leading edge the WC coating over that area will be worn down. After the coating has been worn completely the hammer will be rotated so that the top right will be the leading edge.

Figure 2.10: Tungsten carbide coated hammer for a hammermill [43]. The coating can be seen on the edge of the hammer on the right side of the image.

Conveyor systems experience wear in components such as the chains, gliding rails and wear pads. Screw conveyors can also be a site of both mechanical wear and fuel adhesion problems. This can be of particular importance due to the role screw conveyors play in some biomass power plants. Screw conveyors are often used to inject the biomass fuel into the boiler, and so any stoppage of the screw conveyor could potentially result in power production to stop. This makes uninterrupted operation of the fuel feeding screw conveyors of higher importance when compared with other sections of the fuel handling

systems at power plants, and economic losses associated with downtime of these screw conveyors can be larger.

2.3.3 Energy conversion/fuel combustion

The primary needs for improvement in the fuel combustion stage are the prevention of the formation of ash deposits and corrosion inside the boiler. No solution is currently available to completely remove either problem. Ash deposits require periodic cleaning, often using concentrated steam jets. Corrosion of surfaces leads to periodic replacement of boiler components. [15]

As mentioned in section 2.1.3.3 the NO_x and SO_x emissions from biomass burning power plants are generally lower than those of fossil fuel burning power plants. There are also primary and secondary emission reduction methods which can be used to further lower the release of these chemicals. Reduction in cost of these emission reduction methods would improve the economic competitiveness of biomass fueled power plants. Biomass combustion is considered to be CO_2-neutral with respect to CO_2 concentrations in the atmosphere due to the CO_2 which is released during combustion having been adsorbed during the life of the biomass. However, cost effective CO_2 capture methods could allow biomass combustion to have negative net atmospheric carbon emissions [44]. This would further improve biomass combustion's position as an environmentally friendly energy source.

Biomass combustion can lead to rapid deactivation in the catalysts used in SCR to remove NO_x. This problem can be seen in pure biomass fired plants as well as coal/biomass co-fired plants. The causes of the deactivation are numerous and vary depending on the fuels being used. In a biomass only fired boiler potassium salts present in the biomass were the primary cause of catalyst poisoning and the biomass ash was more likely than coal ash to deposit onto the surfaces of the SCR system causing a drop in performance [45]. Zinc salts were also shown to cause deactivation in the SCR catalyst [46]. Strege et al. [47] reported that in a co-fired plant using a combination of tree bark and saw dust deactivation of the SCR catalyst occurred rapidly. The cause was determined to be that "alkali and alkaline-earth metals from the biomass formed layers of sulfate where ash deposited near catalyst pores" [47].

Two problems that have been observed to occur on grate boilers are: wear on the grate and ash deposits on the grate. All grate boilers involve movement of the fuel from the place of fuel injection to the point of ash removal. This can occur through many different mechanisms as mentioned in section 2.1.3.1. Wear can occur on the grate in any of these situations as the fuel moves relative to the grate. Ash deposits can also form on the grate surface which can hinder the movement of the fuel and cause uneven combustion across the grate.

2.3.4 Waste heat recovery

Condensing turbines are the most common type of steam turbine used in electricity production. For power plants using condensing turbines the condensate formed from the steam in the condenser is a large source of waste heat when it is exhausted to the environment. If a power plant uses a cooling tower the temperature of the inlet water of a cooling tower is generally the same as condensate in the steam condenser. To give an idea of the temperature ranges being dealt with for this type of waste heat, the cooling water at the inlet of the cooling tower can be assumed to be between 35-50 °C.

Flue gas exhaust can also be a source of lost energy during power production. If flue gas condensation is used by the power plant then the temperature of the condensate is below the dew point of the flue gas. This can be assumed to be around 50 °C. If flue gas condensation is not being used then implementing it would most likely be the best first step to improving overall efficiency.

In both the case of condensed steam and condensed flue gases the temperature of the condensate is higher than the ambient air temperature to which it will be exhausted. This temperature difference could potentially be used to capture some of the wasted energy of the power production. [15]

2.4 Nanotechnology solutions

Nanoscience has offered solutions to problems in numerous different industries and power generation is no different. Nanoscience is, however, a relatively new field of study. Many nanoscience advancements are still confined to laboratory tests or too expensive to see wide spread use, but this will change over the next few year as the technologies mature. Sections 2.4.1 through 2.4.4 review some nanoscience solutions to the problems discussed in section 2.3.

The technologies presented in sections 2.4.1 through 2.4.4 can be considered nanotechnology for a variety of reasons. In general these technologies fall into one of three categories: nanolayers or thin films, nanocomposites and nanostructured materials. Nanolayers and thin films refer to coatings which have a depth of less than 100 nm. Thin film can also refer to layers which have a thickness of up to several micrometers, though its usage here is restricted to layers of nanometer scale. Nanocomposites are solid materials with two or more phases where at least one phase has structures on the nanoscale, or there are dimensional repeat distances of the nanoscale between the phases. Nanostructured materials is a general term for any material with features on a nanometer scale. These features can be one, two or three dimensional which would refer to nanostructured surfaces, tubes and particles respectively. [48]

2.4.1 Coatings

The coatings discussed in this section will be limited to nanolayer coatings and thin films, those which have a size of less than 100 nm up to a few micrometers, and nanostructured coatings, those which may be of any thickness but gain their properties from nanosctructures in the coating material. Some coatings can be applied using certain thermal spraying techniques, such as plasma spraying and high-velocity oxy-fuel coating spraying. Other coatings, often thin films, must use techniques such as sputtering, pulsed laser deposition or molecular beam epitaxy. In general, thermal spraying techniques are significantly more convenient for large scale application as they can be applied to comparatively large areas. A summary of the coatings discussed in this section is given in Tables 2.1, 2.2 and 2.3.

Table 2.1: Nanocoatings which have a primary purpose of wear resistance or low friction.

Material	**Nano feature**	**Deposition method**	**Function**	**Reference**
Al_2O_3-13TiO_2	Nanopowder feed	plasma spray	Wear resistance	[49], [50]
Cr_2O_3-5SiO_2-3TiO_2	Nanopowder feed	Plasma spray	Wear resistance	[49]
TiO2	Nanopowder feed	Plasma spray	Wear resistance	[49]
Al_2O_3-13TiO2 + CeO_2	Nanopowder feed	Plasma spray	Wear resistance	[50]
Al_2O_3-13TiO_2 + CeO_3 + ZrO_2	Nanopowder feed	Plasma spray	Wear resistance	[50]
Yttria-stabilized zirconia (YSZ)	Nanopowder feed	Plasma spray	Wear resistance	[51]
SHS7170	Crystallites with sizes ranging from 60 to 140 nm	wire-arc coating	Wear resistance	[52]
WC / WC-Co	Nanopowder feed	plasma, HVOF spray	Wear resistance	[53], [54]
Nanocrystalline diamond	Average grain size $<$ 100 nm	CVD	Wear resistance	[55]
Diamond-SiC composite	Nanoscale SiC matrix	High P–T sintering	Wear resistance	[56]
Boron-aluminum-magnesium (BAM)	Nanostructured composite alloy	Pulsed laser deposition, magnetron sputtering	Wear resistance, low friction	[57]
Ni–ZrO_2	ZrO_2 particles 10-30nm	Electrodeposition	Wear resistance, low friction	[58]

Table 2.2: Nanocoatings which have a primary purpose of corrosion and oxidation resistance.

Material	**Nano feature**	**Deposition method**	**Function**	**Reference**
Ni-Al_2O_3	Al_2O_3 particles mean diameter 100 nm	Sediment co-deposition	High temperature oxidation and corrosion protection	[59]
SiCN composite	Nanoscale SiCN matrix	Magentron sputtering	Wear resistance, oxidation resistance	[60]
TiB_2	Nanoscale matrix	Magentron sputtering	Wear, abrashion, high temperature corrosion and oxidation resistance	[60]
TiAlCrSiYn	Nano-crystalline	Plasma vapor deposition	High temperature oxidation protection	[61]
Cr_3C_2-25(Ni20Cr)	Average carbide particle size 20-70 nm	HVOF	High temperature corrosion and oxidation protection	[62], [63]
CeO_2	Ceria particles 3-5 nm	Dip coating	High temperature oxidation protection	[64]
Fe-Cr-Ni-Al	Grain size 60 nm	Magnetron sputtering	High temperature oxidation protection	[65]
SHS 7570	Nanoscale grain size	TWAS	High temperature corrosion protection	[66]
Ti3Al(O)-Al2O3	Nano composite	Thermal spraying	High temperature oxidation protection for Ti alloys	[67]

2.4.1.1 Mechanical wear resistant coatings

One of the primary concepts in wear resistant nanostructured coatings is the inverse relationship between grain size of metals and yield strength, or hardness. This relationship is expressed by the Hall-Petch relation given by equation 2.3,

$$\sigma_y = \sigma_i + k_y d_g^{-1/2}, \tag{2.3}$$

where σ_y is the yield strenght, d_g is the grain diameter, and σ_i is generally interpreted as the lattice friction. The final term, k_y is a constant referred to as the strengthening coefficient, though its physical interpretation is less well defined [70]. As σ_i and k_y are both constant for a material under the same conditions, the yield strength will increase as the grain size decreases. There is a size limit to application of the Hall-Petch relationship however, as Zhao et al. [71] reported that below grain sizes of the 15-30 nm range the relationship no longer holds.

Carbodeon, a Finnish company based in Vantaa, supplies coatings for increased toughness. uDiamond is a coating material composed of nano-diamond particles. These particles are of the size range 4-6 nm. One version of the product is suitable for use in

Table 2.3: Nanocoatings which have a primary purpose of anti-icing.

Material	**Nano feature**	**Deposition method**	**Function**	**Reference**
SiO2-polyerm composite	SiO2 nanoparticles	Spray gun	Superhydrophobic/ anti-icing	[68]
ZrO2-polyerm composite	ZrO2 nanoparticles	Spin coating	Superhydrophobic/ anti-icing	[69]
Ag-polyerm composite	Ag nanoparticles	Spin coating	Superhydrophobic/ anti-icing	[69]

electrolytic coatings. Coatings made from nanodiamond powders have been shown to improve hardness and wear resistance [72].

Oerlikon Balzers also offers a series of coatings under the brand name BALINIT designed to increase hardness. The coatings are generally marketed towards small scale applications, such as cutting and machining tools. These coatings use titanium nitride, aluminium chromium nitride, chromium nitride and other materials. They have a wide range of maximum working temperatures from 600 °C to 1200 °C. In mass production the coatings can be between 0.5 and 4 micrometers thick. One of these coatings, BALINIT FUTURA NANO, is specifically marketed as being a nanostructured coating with good abrasion and wear resistance.

Multiple studies have been done on wear resistance of plasma sprayed nanocoatings [50][73]. Chawla et al. [49] describes the findings of a number of these studies in which Al_2O_3-13TiO_2, Cr_2O_3-5SiO_2-3TiO_2, TiO_2 and other nanostructured powders were used to produce coatings. It was concluded from these that plasma sprayed coatings using nanostructured powder feed could provide improved wear resistance over other forms of thermal spray coatings. Other studies on plasma sprayed nanostructured zirconia [51]nd WC–Co [53] coatings report that the nanostructured coatings exhibit better wear resistance properties than the conventional counterparts. In both studies both nanopowders and conventional powders were used as feedstock for the spraying process. In the case of the zirconia nanopowder the average particle size ranged from 70-110 nm and these particles were then reconstituted into micrometer sized spherical particles before the plasma spraying. The convential zirconia powder particle size was 1-5 μm. It was reported that the nanostructured coating had a wear rate of less than half of that of the conventional coating under loads of 20 N to 80 N. The WC-Co coating was also applied using plasma spraying, and the nanopowder particle size was approximately 35 nm while the conventional particle size was 10 μm. The nanostructured WC-Co coating had a wear rate of less than one-sixth of the conventional coating under loads of 40 N to 60 N.

Some applications require coatings physical properties beyond normal wear resistance and coatings with extremely high hardness and toughness are needed for these situations. For example, the leading edge of the hammers used in hammermills to grind tree stumps

as described in sections 2.1.2 and 2.3.2 use tungsten carbide coatings. These WC coatings can be made to be one mm or more in thickness which allows for increased life in high wear environments. According to Zhang et al. [74] 'superhard' materials are with a hardness of greater than 40 GPa. These superhard coatings could replace currently used coatings in demanding applications such as hammermills. Creating superhard nanomaterials is an area of significant research, though Zhang reports that the toughness of the materials has in general not kept pace with the increasing hardness which has limited the applications to which these materials are currently suitable. Finding ways to avoid the decrease in toughness which typically accompanies an increase in hardness is one of the goals of nanoscience research into superhard materials.

Some WC coatings formed from nanopowders have already been discussed as showing improved characteristics when compared with conventional WC coatings [53], and this may be used to improve hardness and toughness of WC coatings further. Wear properties of nanostructured WC coatings have also been studied with varying results. Stewart et al. [54] found that nanocomposite HVOF-sprayed WC–Co coatings had diminished wear resistant properties compared with the conventional coating. The study concludes that the "increase in wear rate is attributed to the greater degree of decomposition suffered by the nanocomposite powder particles during spraying which leads to a reduction in the volume fraction of the wear-resistant primary WC phase and the formation of brittle amorphous binder phases within the coating." In a study of plasma sprayed WC coatings Zhu et al. [53] found that the nanostructured coating had improved wear resistant properties compared with their conventional counterpart. The use of diamond coatings on tungsten carbide has also been investigated by Meng et al [55]. In this study the average grain size of the diamond film was less than 100 nm and it gave increased hardness and wear resistance to a WC-Co drill.

The NanoSteel Company offers near nanoscale coatings which have hardness and toughness measurements exceeding those of WC. The coatings are reported to have a surface structure on the scale of 400 nm, but shows the trend towards nanoscale structures and improved physical properties. Many of these materials can be applied in coatings up to 2.5 cm thick. Many of the coatings have been developed to provide erosion resistance at high temperatures, some were designed specifically for use on boiler tubes. Branagan et al. [52] described one such coating from The NanoSteel Company using an iron base. The coating was applied using a thermal spray technique, the wire-arc process. During the spraying processes the coating material forms nanoscale micro structures which give the coating its improved properties.

A summary of the hardness and toughness values reported in the literature for a variety of nanostructured materials is presented in Table 2.4. The values for conventional WC-Co is given first in the table for comparison purposes. It can be seen from the table that the conclusions of Zhang et al. appear largely accurate; there are many nanostructured

Table 2.4: Common hardness and toughness measurements for various materials.

Material	**Vickers Hardness in GPa**	**Palmqvist fracture toughness**
Conventional WC-Co	11-20 [75]	12-15,3 $MNm^{-3/2}$ [76]
Nanostructured WC-Co	17-24 [77]	8-8,5 $MNm^{-3/2}$ [77]
Nanostructured WC/DLC	27 [78]	Not reported
TiN/a-Si_3N_4	50 [79]	Not reported
Nanostructured diamond-SiC composite	60-80 [56]	12,5 $MNm^{-3/2}$ [56]
SHS 7214	6-7 [66]	55 $MNm^{-3/2}$ [66]
SHS 9290	11-14 [66]	Not reported

superhard materials which have hardness much greater than conventional materials, but the as of yet inability to break the inverse relationship of hardness and toughness have limited the applications of these nanostructured materials. Nanostructured diamond-SiC composite as described by Zhao et al. [56] is one of the few examples of a coating which has achieved both superhardness and high fracture toughness and shows that the tradeoff between these two properties is avoidable. It should be noted that the reported hardness values for different materials are not always directly comparable due to differences in test setups and measurement techniques. However the values still give an accurate idea as to the trends of the hardness and toughness values for nanostructured coatings.

2.4.1.2 Anti-friction coatings

Anti-friction coatings are often related to mechanical wear resistance, as it is often desired to have a coating which is both high in wear resistance and possessing a low coefficient of friction. The BALINIT coatings produced by Oerlikon Balzers mentioned in section 2.4.1.1 also have improved coefficient of friction values, between 0,1 and 0,5 against dry steel. Steel has a coefficient of 0,78 and polytetrafluoroethylene (Teflon) 0,04 in similar conditions.

Nano-layer coatings can also offered lower coefficient of friction values. Yamamoto et al. [80] reported that a multilayer coating of chromium nitride (CrN) and boron carbo-nitride (BCN) had a coefficient of friction of 0,2. In that case the CrN layer was 20-100 nm thick and the BCN layer 1-5 nm. Tungsten carbide reinforced nickel-phosphorus (NI-P-WC) nanocomposite coatings have also been shown to exhibit impressive tribological and hardness properties [81], as have polymer nanosheets [82].

Aluminium magnesium boride is a ceramic alloy that is of great interest in low friction, wear resistant coatings. It has been reported to have a coefficient of friction ranging between 0,02 and 0,1 while its hardness value is between 29 and 32 GPa. This gives a

hardness potentially greater than tungsten carbide and a coefficient of friction potentially lower than Teflon. [57]

2.4.1.3 Anti-icing coatings

Anti-icing materials have a wide range of applications and have consquently been under research for many years. De-icing and anti-icing fluids have been used heavily in the airline industry since the 1980s [83]. While research into anti-icing materials takes place in a variety of fields, recently superhydrophobic materials have become a topic of major focus. These materials repel water to such an extent that the water will form a ball and roll off the surface which can prevent the water from freezing to the surface. Superhydrophobia has shown to be effective at preventing ice formation, or at least reducing the adhesion force of ice to the material surface, in a number of studies [69] [68]. However, Kulinich et al. [84] showed that superhydrophobic materials are not necessarily ice repellent and testing of hydrophic coatings in 1997 [85] also showed that hydrophobicity does not necessarily correlate to icephobicity. Figure 2.11 shows an aluminum plate which has one side coated with a superhydrophobic composite and a satellite dish which also has one side coated with the same composite. The other side of both objects was left uncoated and the two objects were left outside for one week, during which time there was naturally occurring freezing rain. It is clear that the sides which have been coated in the superhydrophobic composite have little, if any, ice while the uncoated sides are largely covered.

Recently Varanasi et al. [86] showed that while some superhydrophobic materials can prevent liquid water from freezing onto the surface they cannot prevent water vapor from depositing as ice onto the surface. Ice deposited in this way is typically called frost. It was shown that frost was able to form over all areas of superhydrophobic materials, and once frost had formed on the surface the material lost its superhydrophobic properties. Figure 2.12 shows a water droplet impacting on a dry and a frosted superhydrophobic surface. The dry surface was maintained at room temperature, 18 °C, and the frosted surface was at -5 °C. On the dry surface the water droplet is repelled and recoils whereas on the frosted surface the water wets the surface and then freezes. This potentially causes a major setback for superhydrophobic anti-icing coatings to be used in real world applications in the near future. Studies on important properties such as wear resistance are also not yet available on these superhydrophobic coatings.

2.4.1.4 Anti-corrosion coatings

A 2007 review of nanostructured coatings for boiler tube corrosion prevention was conducted by Grandy [27] at the Electric Power Research Institute (EPRI). The results of the study are, however, of limited application to biomass boilers due to the focus on coal-fired power plants. The corrosion in these coal-fired power plants was caused primarily by sulfur which is not the corrosive agent common to biomass, as discussed in

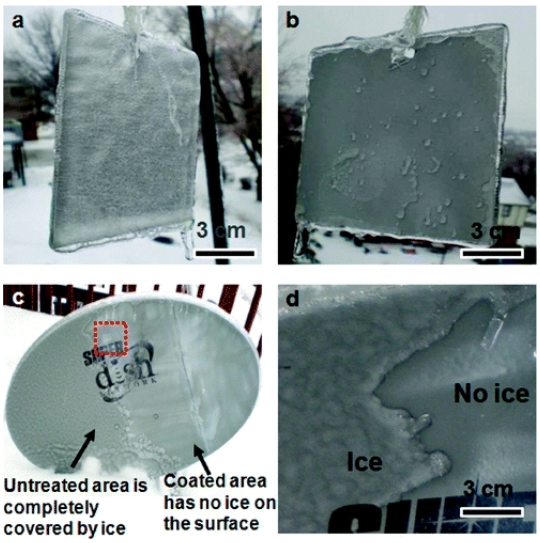

Figure 2.11: Anti-icing coatings: images a and b show the uncoated and coated sides respectively of a aluminum plate, images c and d show a satellite dish with half of the surface coated in the same anti-icing coating [68].

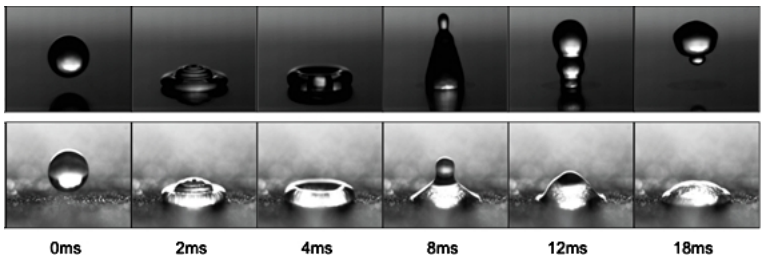

Figure 2.12: (a) Water droplet impacting on dry superhydrophobic surface. (b) Water droplet impacting on frosted superhydrophobic surface [86].

section 2.1.3.2. Chlorine corrosion, the corrosion of greatest concern to biomass boilers, was discussed in the EPRI study but was not given as strong of consideration as sulfur corrosion. The conclusion of the study was that certain nanostructured coatings which contain aluminum or chromium have better corrosion resistant properties than the conventional counterparts. This improved corrosion resistance comes from the formation of oxide scales of Al_2O_3 or Cr_2O_3 which have better adherence and spalling resistance than oxide scales on conventional coatings. The nanostructured coatings also require less chromium and aluminum to achieve the same corrosion resistance.

There are a variety of nanostructured materials which have been shown to provide oxidation resistance. Nano-crystalline TiAlCrSiYn coatings were shown to develope continuous protective oxide scales, giving improved oxidation resistance at 900 °C [61]. The coatings also showed improved wear resistance and also exhibited self healing properties. However, as mentioned in section 2.1.3.2, these scales have in some cases proven less effective in protection from corrosion in high chlorine environments. Sundararajan et al. [64] studied 9Cr–1Mo ferritic steel coated with nanoceria under high temperature

oxidizing conditions. The ceria nanoparticles were 3-5 nm and steel was coated using a dip process. The coating thickness was 150-200 nm. Tests at 650 °C showed the coating improved oxidation resistance while showing less mass gain and a four to fivefold reduction in the thickness of the oxide layer. Fe-Cr-Ni-Al nanocrystalline coatings [65] have also been shown to form Al_2O_3 scales under oxidizing conditions and provide improved protection at 800 °C and 900 °C. The coating was deposited using magnetron sputtering onto AISI 310S stainless steel. Other studies have continued to show the benefits of using nanocoatings rather than conventional coatings for corrosion protection, however there has been little work done in the corrosion conditions of biomass boilers. In all of these cases tests in high temperature chlorine containing conditions must be done before the coatings could be considered for use in real world bioenergy applications.

Current research into coatings for anti-corrosion in high temperature, chlorine rich environments is limited. However, VTT and Aalto University were recently awarded the Best Result in DEMAPP in 2010 at the Annual Seminar of the DEMAPP Program for their work in this area. The results are currently unavailable to the public. [87]

A nano-coating developed at Brookhaven National Laboratory has been reported to potentially provide an alternative to chromium for use in anti-corrosion of metals. The coating is a thin film of less than 10 nm and can be applied to steel, along with a variety of other metals [88]. Published performance results of the coatings in a chlorine environment were not yet available.

The NanoSteel Company offers a variety of nanostructured thermal spray coatings for use on steel. These coatings are iron based steel alloys with up to 25% chromium. They can be applied using a variety of thermal spray processes and have a microstructure grain size of 10-100 nm. The coatings are advertised to protect against chlorine corrosion and for use in woody biomass CFB boilers, however no independent assessment of the effectiveness of the coatings in these situations was available. [66]

2.4.2 Nanostructured steel

Improving the properties of the bulk steel itself is a wide and ongoing field of research and could potentially eliminate the need for coatings in some situations. One of the primary methods of improving the strength and corrosion resistance of steel is grain size refinement. In commercial steels a grain size of 5-10 μm is common, while recently it is become possible to produce ultra-fine grain steel with grain size of 1 μm or less [89]. Continuation of this grain size reduction into the nanometer scale is also under investigation and has already been met with some success [90]. The primary limiting factor in preventing steels of ultra-fine and nanoscale grain size from becoming commercially available is the decrease in ductility which accompanies decrease in grain size. It has been proposed that metallurgical approaches and changes to the microstructure of the steel may be able to reduce this [91].

2.4.3 Flue gas cleaning and emission reductions

Nanotechnology methods for cleaning of flue gases and reduction of emissions can be put into two general categories. The first is filters and membranes. These do not involve chemical reactions but simply physically separate the constituents of the gas or liquid which passes through the filter or membrane. Catalysts, on the other hand, remove chemicals by affecting the rate of chemical reactions.

2.4.3.1 Filters and membranes

Development of methods to remove CO_2 from power plant emission is a large field of research. While fossil fuel based power plants may have the most pressing need for CO_2 capture, most technologies can also be used for biomass based power plants. Membranes have been available for separating CO_2 for many years, but they require high pressures to function efficiently and are therefore ineffective with flue gases from a biomass plant. Nanomembranes, nanostructured membranes which separate substances at a molecular level, could provide a way to overcome this limitation. Nanomembranes against Global Warming (NanoGLOWA) is a research group funded by the European Commission and is currently doing tests on a number of different membrane types. The project is expected to finish in 2011. One of the member groups of NanoGLOWA, the MEMFO group at the Norwegian University of Science and Technology, was issued a patent in 2007 for a nanostructured membrane for use in CO_2 capture. A group at University College Dublin has also developed a nanoporous membrane which can separate CO_2 from nitrogen with a selection rate of 75:1 at 873 K [92]. This membrane was 5-25 nm in thickness and composed of silica. The membrane was deposited on a Vycor® microporous glass tubing substrate using chemical vapour deposition.

2.4.3.2 Catalysts

Nanotechnology has already been incorporated into commercial catalyst products. One example is a catalytic converter used by Mazda, in which the use of nanoparticles to increase the effective surface area of the precious metals used and thereby reduce the total amount of precious metals needed by 70% [93]. Reduction of precious metal usage is an application of nanotechnology that can be used anywhere catalytic converters are needed, though this is not the limit of the potential uses of nanotechnology. The ability to design the catalyst on atomic level will allow for increases in selectivity, efficiency, operational temperature ranges, and other important properties. Nanocatalyists have already been shown to have potential in removal of sulphur and NO_x from power plant emissions [94] [95].

Regarding the poisoning of SCR catalysts by the potassium and zinc salts, more work must be done to find solutions to these problems. New nanostructured catalysts are being

developed which have shown to have good properties for NO and N_2O reduction, though no information is available on potassium poisoning for these [96][97].

2.4.4 Waste heat recovery

Compared with a power plant which produces only electricity a CHP plant has relatively little wasted energy. The energy that is lost is done so when the flue gas, condensed steam or cooling water is exhausted to the environment. As stated in section 2.1.4, flue gas condensation is one of the most cost effective ways to improve energy recovery in a biomass power plant. Neither of the potential nanotechnology solutions to waste heat recovery will replace flue gas condensation as the first choice in energy recovery for many years to come, if ever. If flue gas condensation has already been implemented, the flue gases will exit below the dew point temperature. The same is true for condensed steam. This means that most of the lost energy from a CHP plant will be from low temperature exhausts, making waste heat recovery difficult. Two nanotechnologies which may be of use for waste heat recovery are thermoelectrics and thermophotovoltaics.

2.4.4.1 Thermoelectrics

Thermoelectrics offer the ability to directly convert a temperature differential into electricity. The thermoelectric effect which is used to produce the electricity from the temperature difference has been known for decades and research in the field has continued since at least the 1950s. However, the efficiency of the conversion process remains too low for thermoelectrics to see widespread use. Nanoscience offers a variety of new possibilities to increase the efficiency of thermoelectrics high enough so that they may begin to see use outside of the few specialty applications to which they are currently limited. [98]

The primary method used to determine the efficiency of a thermoelectric material is the 'figure of merit' value. The figure of merit is defined as

$$Z = \frac{\sigma S^2}{\kappa} \tag{2.4}$$

where σ is electrical conductivity, S the Seebeck coefficient and κ is the thermal conductivity. Multiplying Z by the average temperature at which the device operates gives a dimensionless figure of merit, ZT. A ZT value of 1 corresponds to operating at 10% of the Carnot efficiency at the same temperature, while a ZT of 4 is approximately 30% of the Carnot efficiency. For bulk thermoelectric materials ZT has increased from approximately 0,6 to one over the past 50 years [98]. It is widely thought that a ZT value of greater than 4 would allow thermoelectrics to see widespread use. Figure 2.13 shows typical figures of merit for a variety of thermoelectric materials over a range of temperatures which may be experienced in waste heat recovery situations.

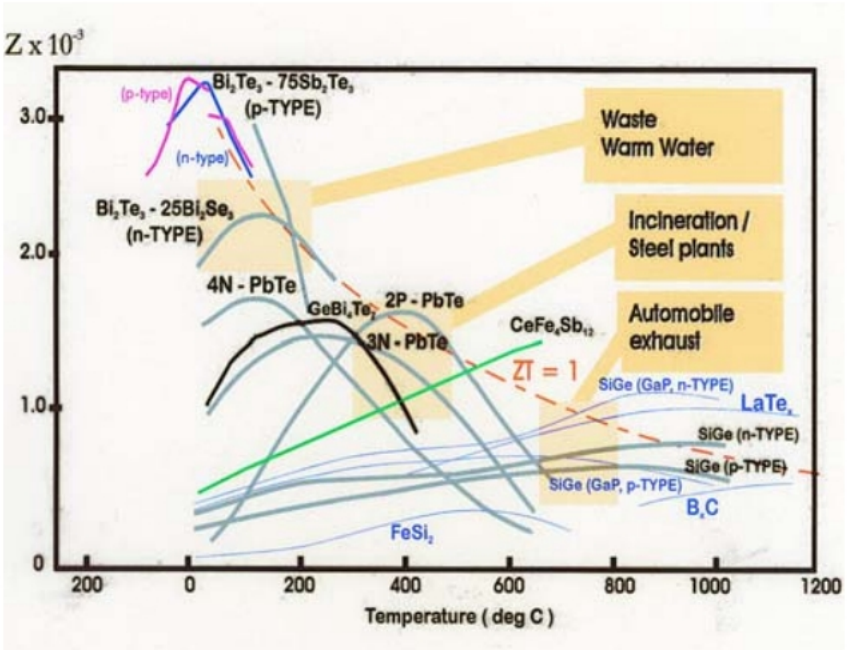

Figure 2.13: Figures of merit for a variety of thermoelectric materials [99].

Much of the nanoscience research done so far on thermoelectrics has been done on superlattices, which are simply periodic structures made up of layers of different materials. Each layer of a superlattice is usually less than 10 nm in size. Harman et al. [100] reported that superlattice thermoelectrics made from PbSeTe/PbTe had a figure of merit ranging from ZT = 1,6 at 300 K to ZT = 3 at 550K. These tests were done on small scales however, and the problems with developing a large scale energy conversion system based on these materials could still be significant. Hochbaum et al.[101] reported that silicon nanowires exhibited a ZT = 0,6 at room temperature. Silicon nanowires have the advantage over some other nanostructured thermoelectric materials in that they can potentially be cheaper and easier to produce in large quantities. However, even taking into account lower production costs silicon nanowires must still have higher conversion efficiencies to be viable for widespread use. Nanocomposites offer a third area of thermoelectric research [102]. Like silicon nanowires, the main attraction to nanocomposites is their ease of production on a large scale when compared with superlattice materials.

Currently there are few commercial systems using thermoelectrics to generate electricity from biomass combustion. Most systems that are available are very small in scale, using thermoelectrics to power fans which allow for more complete combustion of the biomass [103] or better heat flow through the room in the case of a furnace. Champier et al. [104] reported on the possibilities for thermoelectric power generation on biomass cooking stoves, focusing on cooking stoves for use in developing countries. The thermoelectric modules were bismuth telluride and an output of 6 watts was determined to be experimentally achievable. Nuwayhid et al. [105] studied the performance of commercially available small scale thermoelectric systems used with a woodfired stove. The units were

cooled with a heat sink but no fan was used to move air through the sink. A maximum steady state output of 4,2 W was achieved with a single thermoelectric module. A higher output could be achieved using multiple modules though the individual module efficiency dropped in these cases.

Ota et al. [106] reported that in an industrial furnace thermoelectrics were able to achieve a electricity generation efficiency of 7,5% with a temperature differential of 564 K. Larger scale demonstration projects have been setup, but these are rare. Kajikawa [107] describes a 1 kW thermoelectric system attached to the gas exhaust system of a 500 kW diesel co-generation system as well as a thermoelectric system connected to a waste incinerator. The thermoelectric system on the diesel generator was reported to have a thermoelectric conversion efficiency of 5,4% and a total system efficiency of 3,4% [108]. A larger 3 kW system was reported to have an overall system efficiency of 4,30% and thermoelectric modules generated a maximum power output of 3,4 kW [109].

The maximum power output of a thermoelectric system is determined by the thermoelectric material, the number of thermoelectric modules and the temperature difference. The total power produced can be increased by adding more thermoelectric modules to the system. A way to measure the maximum theoretical power generation potential of a thermoelectric system is by examining the total area available to the thermoelectric system and the power density of the thermoelectric materials. The power density is often reported as the maximum power output divided by the area of the hot surface of the thermoelectric. The thermoelectric generators offered by Custom Thermoelectric [110] have a average power density of 0,41 W/cm^2 while Nextreme [111] offers thermoelectrics with an advertised maximum power density of 0,87 W/cm^2. Laboratories studies have shown densities of over 3 W/cm^2 [112][113].

2.4.4.2 Thermophotovoltaics

Thermophotovoltaics, like all photovoltaics, converts photons directly into electricity. The difference between thermophotovoltaics and the more common solar cell photovoltaics is that the photons which the thermophotovoltaics are using to produce electricity are emitted from objects at a much lower temperature than the sun, and so they are of longer wavelength. A thermophotovoltaic system consists of a radiator, heated by some heat source, and the thermophovoltaic cells. Ideally the radiator and thermophotovoltaic cells would be chosen so that the peak emission of the radiator would match the peak absorption of the thermophotovoltaic cells. Even if the emission spectrum of the radiator is well matched with the absorption spectrum of the photovoltaic cell there will still be some emitted photon of too low energy to be absorbed. A filter can remove these sub-bandgap photons and return them to the radiator. Figure 2.14 shows an example of a thermophotovoltaic system which includes a heat source, radiator, filter and thermophotovoltaic cell.

The radiator temperature for these systems can range from less than 1000 °C up to 2000 °C. The necessity of using a radiator in this temperature range means that the current range of uses for thermophotovoltaics is more limited than those of thermoelectrics. Co-generation of heat and electricity and recovery of high temperature waste heat are both still feasible applications [114] [115]. Thermophotovoltaic systems are already commercially avaible for small-scale home use. The Midnight Sun system is a propane burning furnace which generates electricity through thermophotovoltaic panels and is shown in figure 2.15. The system can produce 7500 W of thermal energy and 100 W of electricity [116] [117].

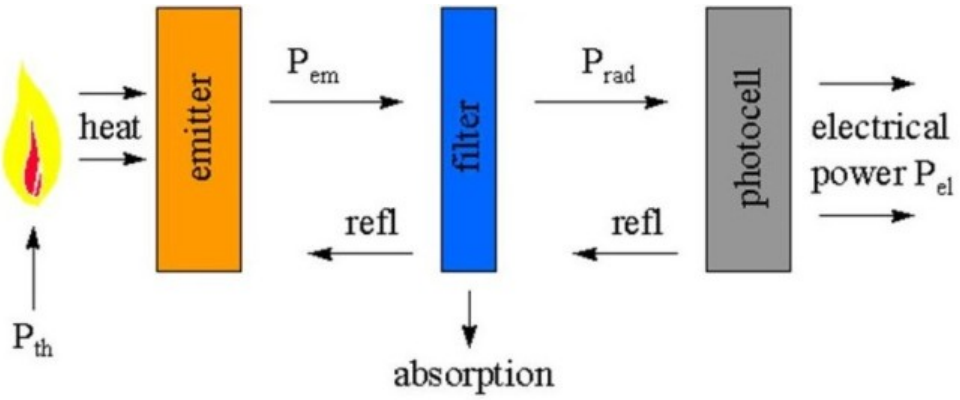

Figure 2.14: Schematic diagram of a thermophotovoltaic system [118].

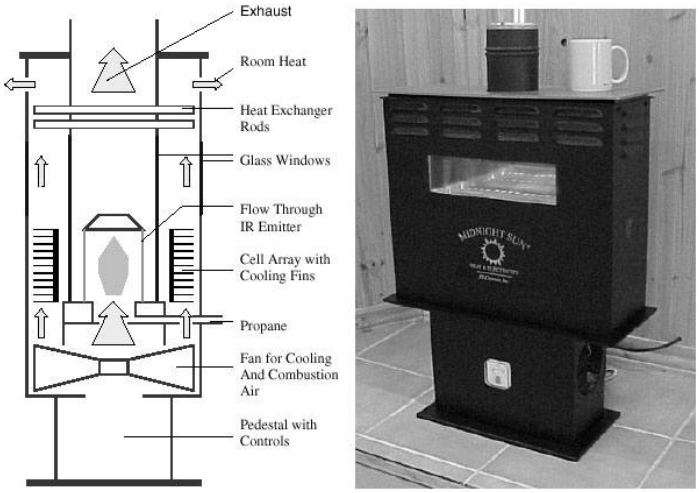

Figure 2.15: A commercially available propane stove and thermophotovoltaic system with a schematic of the interior [116].

Nanoscience plays a similar role in thermophotovoltaics as it does in solar cell research by allowing for new materials with better absorption and emission properties. The materials used in the thermophotovoltaic cells are designed to have a very specific band gap absorption and emission spectrum and to operate at specific temperatures. Lowering the

operating temperature of the systems would also improve the compatibility with biomass combustion, as temperatures inside both home fireplaces and large biomass boilers tend to stay well below 1000 °C. There has been some progress in this area, as Nagpal et al. [119] reported that metallic photonic crystals had been used as a thermophotovoltaic emitter operating near 650 °C. Superlattice materials are another common way of obtaining highly specialized band gap at lower temperatures. A GaAsN/InAsN superlattice matched to InP has been shown to have the potential of a band gap in the range 0.7-0.35 eV [120], which corresponds to the peak emission wavelengths of a backbody between the temperatures 525 °C and 1475 °C. Designing the radiator of the system to emit a more narrow spectrum than would occur from a typical blackbody has also been a topic of much research. Quantum wells, superlattices and nanocrystals all offer some potential in this role [121]. Nano-ethching of an p-GaSb emitter has also been shown to offer efficiency improvements [122].

The primary focus thermophotovoltaic system design has been small scale cogeneration, namely home furnaces. Many of these designs make use of the semiconductor gallium antimonide (GaSb) for the thermophotovaltic cell. Most designs use gas or oil fired furnaces [123][124][125], though one design implemented a wood powder furnace [126]. The size of the furnaces which have been designed range from 1,35 kW thermal to 12,2 kW thermal, and they have thermal to electric conversion efficiencies which range from 1,1% to over 30%. There is little reason why similar thermophotovoltaics could not be used on any furnance system, including solid biomass fueled, which reaches appropriately high temperatures.

2.5 Nanofabrication methods

Many materials with nanoscale features require special fabrication methods. This section gives a very brief overview of some of the methods which are required in the fabrication of the materials discussed in section 2.4.

2.5.1 Electrodeposition

Electrodeposition is a coating method which has been in use for over two centuries. The basic principle of electrodeposition involves placing electrodes into a solution containing metal ions. When a current is run through the solution the metal ions are moved to coat the cathode. Electrodeposition can be used to fabricate a variety of nanostructured materials, such as nanowires, nanofilms, multilayered nanocoatings and nanostructured composite coatings. The process also offeres many advantages over other methods such as chemical vapor deposition, such as rapid deposit formation and low cost. Figure 2.16 shows a schematic diagram of the electrodeposition process. [127]

2.5.2 Chemical vapor deposition

Chemical vapor deposition (CVD) is a procedure which can be used in the fabrication of thin films, high-purity bulk materials, powders, composites and other materials. The process, in a simplified form, involves flowing a precursor gas, or gases, through a chamber containing the substrate on which the coating will be deposited. The substrate is heated, and a chemical reaction occurs at the surface of the material which results in the deposition of a thin film. There are numerous variations on this process based on the substrate and precursor gases being used, as well as the desired coating properties. Most CVD techniques require low pressure and high vacuums, however some versions of the process can be performed at atmospheric pressure. Temperatures tend to range from 200 °C to 1600 °C. [128]

The thin films produced by CVD are used for corrosion protection, wear resistance, increased hardness, and other applications. Deposition of diamond coatings is an area of particular research interest. The properties of diamond which make coatings of interest are high hardness, high thermal conductivity, low coefficient friction and its chemical and electronic properties. CVD thin films are widely used to create dielectrics and conducting films in in the semiconductor industry and electronics industries [129], as well as for potential use in solar cells [130]. CVD is also a common process used in the creation of various types of nanowires [131][132][133].

2.5.3 Physical vapor deposition

Physical vapor deposition (PVD) is a general name which refers to a large number of vacuum processes in which the coating material is passed into a vapor transport phase by a physical driving mechanism. Examples of the driving mechanisms are evaporation, sublimation, and sputtering. During the deposition process, the coated sample can often be maintained from ambient to 100 °C while the pressure is usually below 10^{-2} Pa. As the techiques are used for the deposition of a coating onto a substrate, the primary fields of interest are thin films and nanostructured coatings.

The method of vapor formation can have a large effect on the properties of the coating and each vapor formation method can have advantages in certain applications. Deposition by evaporation involves heating the coating material in a vacuum. The coating material will form a vapor and condense onto the substrate. This is shown in Figure 2.17. Sputtering deposition does not heat the coating material to form a vapor, but instead uses high energy particles to transfer kinetic energy to the coating material, or target, in order to remove material for deposition. The atoms which have been removed by the sputtering process then condense onto the substrate, forming the desired coating.

Pulsed laser deposition (PLD) involves the use of a high powered laser, which is focused onto the coating material. This vaporizes material from the target of the laser which then

deposits onto the surface of the substrate material. This process has many advantages over similar techniques such as the large number of materials which can be deposited and the fact that the substrate material can remain at room temperature during the deposition process. PLD has not seen widespread use in large scale industrial and commercial coating applications, however, and it remains largely confined to laboratory applications. PLD could see increased use in large scale coating applications in the future as laser prices drop. Multiple lasers are required to be used simultaneously to achieve high speed coating. [134].

Molecular beam epitaxy (MBE) is a subgroup of evaporative physical vapor deposition. The primary distinguishing characteristic of MBE is the slow growth rates of the thin films, which require a high vacuum. MBE growth chambers usually incorporated a number of analytical instruments, allowing growth of the film to be monitored. The slow growth rate of the film allows the deposition process to be well controlled and the low temperatures which MBE can be operated at are conducive to the fabrication of many nanostructures.

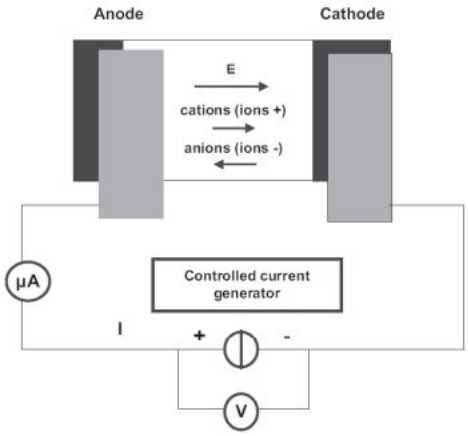

Figure 2.16: Schematic diagram of electrodeposition [127].

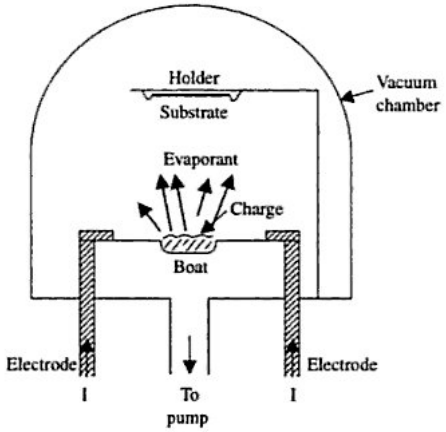

Figure 2.17: Schematic diagram of evaporative physical vapor deposition. The coating material is vaporized using heating unit, and is contained with the substrate inside a vacuum chamber [135].

Physical vapor deposition techniques have been used in commercial and industrial production for many years. PVD has been used in the semiconductor industry for decades, while coated tools and instruments for corrosion and wear protection are relatively common [136]. PVD systems are also used in other electronics production, such as flat screen TV panels [137]. MBE also sees wide use in the semiconductor and electronics industries [138].

2.5.4 Atomic layer epitaxy

Atomic layer epitaxy (ALE), or atomic layer deposition, is a fabrication method similar to chemical vapor deposition. The underlying operational principle is the same as that of CVD with the exception that the precursor gases are pulsed into the deposition chamber

one at a time. In between each pulse of the precursor gases is a purging or evacuation period. This causes at each step a monolayer of that precursor gas to form. ALE has multiple advantages over other nanofabrication methods such as CVD. Thin film growth using ALE has been shown to be effective in relatively large batch sizes as well as having highly accurate thickness control. The primary limitation of the method is the relatively slow growth speed, which is on average 100-300 nm/hour. [139]

2.5.5 Chemical solution deposition

Chemical solution deposition, or sol-gel, is another method which can be used for the fabrication of various nanoscale and nanostructured materials. In the sol-gel process a colloidal suspension, the 'sol', evolves into a gel phase. A drying process is then used to extract the desired product, which could be coatings, powders, fibers, membranes or any number of other materials. [140][141][142]

2.6 Possibilities for relevant nanoscience research at the University of Jyväskylä

The University of Jyväskyä (JyU) has the facilities and capabilities to do research relating to the nanotechnology solutions presented in section 2.4. Much of the research which is possible to do at JyU relates to characterization and analysis of surfaces. This can be done using scanning electron microscopes and atomic force microscopes which are located in the Nanoscience Center. These microscopes can be used for characterization of a variety of materials including nanotubes and nanostrutured coatings. Other simple testing of certain coatings can also be done in the University chemistry laboratories, such as the testing of superhydrophobic coatings for anti-icing properties. X-ray diffraction equipment provides another characterization technique that could be used to study the structure of certain types of coatings.

Nanofabrication methods are also available at the Nanoscience Center of JyU. The university has chemical vapor deposition facilities which, as discussed in section 2.5.2, can be used for deposition of a wide variety of nanostructured coatings as well as the fabrication of nanowires and nanotubes. Nanotubes have a huge range of possible applications are involved in a number of potential solutions discussed in section 2.4. Among other uses, nanotubes synthesized at the Nanoscience Center could be used for testing of thermoelectric properties.

The Nanoscience Center also has facilities for performing ion beam etching (IBE). IBE involves using a beam of heavy, energetic ions to transfer energy to the target material causing ablation of atoms. IBE can be used for surface cleaning and smoothing as well as impregnation of nitrogen in steel. Nitrogen impregnated steel has been shown to have

increased wear and corrosion resistance [143] [144] [145]. The clean and smooth surfaces which IBE can provide may also allow for better adhesion of coatings to the substrate.

Chapter 3

Economic analysis of nanotechnology solutions

The nanotechnology solutions discussed in section 2.4 are in direct response to the areas for improvement in the bioenergy production industry discussed in section 2.3. In nearly every area discussed in section 2.3 there is some nanotechnology that offers significant improvement over the current methods used in the industry. However, in most cases significant obstructions to the widespread adoption of these nanotechnology solutions remain. Cost of implementation is one of those obstructions.

These implementation costs are difficult to know or estimate for a general case. For products that are already in commercial production the prices are often not publicly available and quotes are usually given only in response to specific product inquires from the potential customers. Even in these cases prices are often confidential. Many of the potential nanotechnology solutions are not in commercial production yet, which complicates cost estimation further. Not only can there be unforeseen technical problems when attempting to scale up production of a nanomaterial from the laboratory to commercial scale, but the final cost of the manufacturing process is simply difficult to predict without a detailed study.

As an example of the price differences between conventional and nanostructured materials tungsten carbide powders will be used. A U.S. based company Inframat® Advanced Materials™ LLC is one of the few companies with publicly available prices for nanosized powders. A WC nano powder is sold with an advertised grain size of 40-70 nm and a particle size of 150-200 nm. The price is €175 for 1 kg, which is about 1.8 times the price of WC powder with particle size of 1-2 μm. While this price comparison is not meant to be taken as a general case it does show how the prices can increase quickly for a seemingly small decrease in size.

3.1 Cost estimation framework

Xu et al. [146] have developed a framework for estimating the cost for products incorporating nanotechnology. The framework is very general and the authors do not attempt to quantify the costs for any products, rather a guide for doing the estimation is provided. The authors recommend that industry experts be consulted in order to obtain values for the various costs involved in the estimation. Carbon nanotubes were used as an example and the cost structure for their production was examined in more detail as shown in figure 3.1.

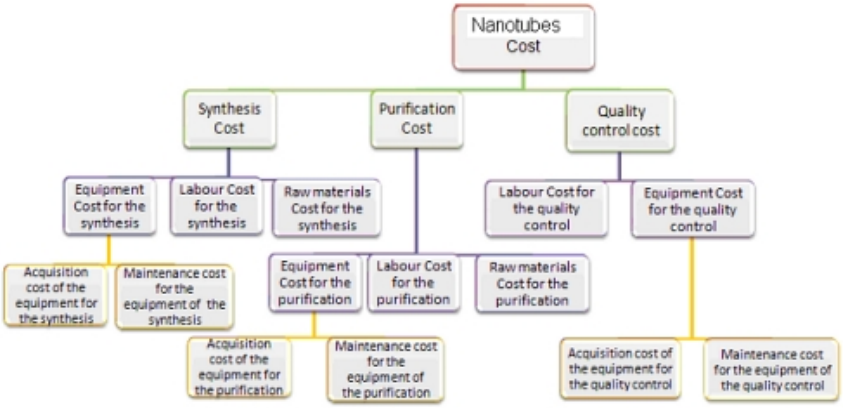

Figure 3.1: Schematic for the cost structure of production of carbon nanotubes [146].

Using the framework provided by Xu as a basis, a breakdown of cost structure of utilizing a nanostructured coating has been developed. Producing a nanostructured coating often involves nanostructured input materials. In many cases, such as nanostructured plasma sprayed WC coatings, at least one of the input materials are nanopowders. In these cases the costs may be largely incurred in the production of the input materials to the coating, rather than the fabrication process itself. In other situations, such as a coating applied with pulsed laser deposition or a method requiring a high vacuum, the fabrication costs can be the primary cost incurring stage.

3.1.1 TiC/a-C coatings

The cost structure for the fabrication of a nanostructured titanium carbide/amorphous carbon coating as described by Pei et al. [147] was examined in more detail. This coating has been applied to steel substrates, making it of particular interest for industrial applications using steel components. The TiC/a-C coating has shown high hardness up to 35 GPa, low wear rates, and a coefficient of friction of 0,04 under dry sliding conditions. A more detailed cost structure is shown in Figure 3.3. The coating process used is magnetron sputtering, a type of physical vapor deposition.

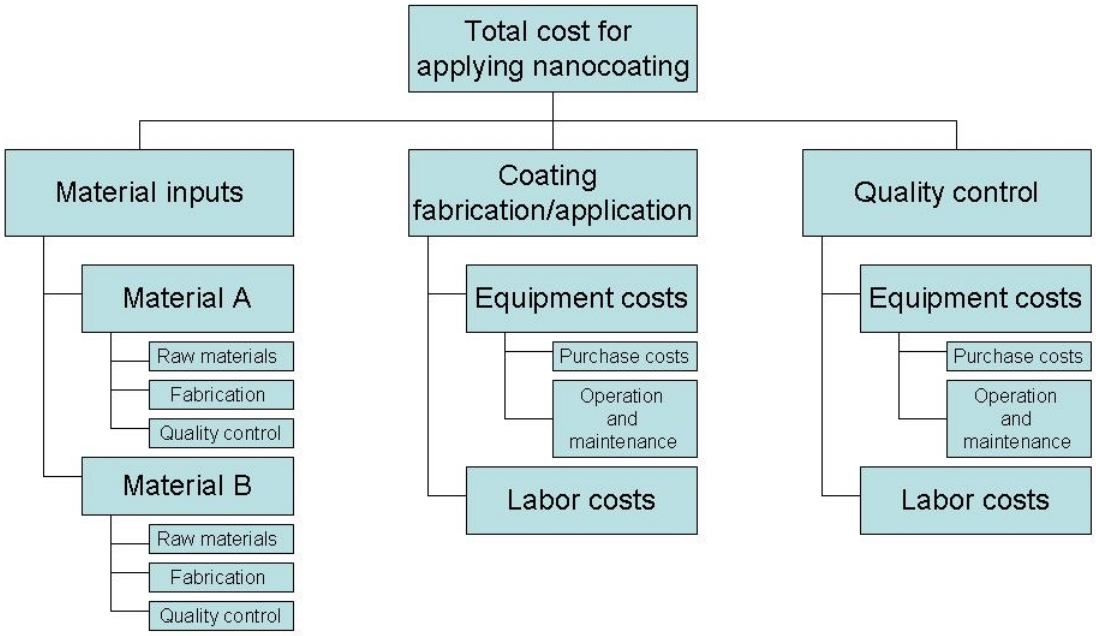

Figure 3.2: Schematic for the cost structure of production for the general case of a nanotechnology [146].

The cost per square meter of surface coated due to the targets was also estimated. While the targets are not generally seen to be the largest contributor to the overall cost of the coating, it is one of the few areas in which an estimate was possible to make. Table 3.1 shows the material makeup and thickness of the coating. The TiC particles are embedded in the amorphous carbon matrix which is estimated to be 5 μm thick based on literature [148] and composed of 30% TiC by volume. The Cr layer is used to improve coating adhesion and is estimated to be 1 μm thick. Other approximations used in these calculations are:

- Target densities are ideal
- Coating densities are: TiC - 4,9 g/cm^3, C - 2 g/cm^3, Cr - 7,2 g/cm^3
- The entire target is deposited onto the substrate.

The costs of the targets and the price per square meter of coating is shown in Table 3.2. The final estimated cost due to the targets is €32 per square meter of surface coated. It should be stressed again that the actual cost to coat a material with TiC/a-C would be much greater as this estimation is a minimum cost for only a single part of the coating process. From Figure 3.3 it can be seen that no costs from the coating fabrication/application or quality control areas have been included in this calculation, as well as the costs of the Argon and acetylene material inputs.

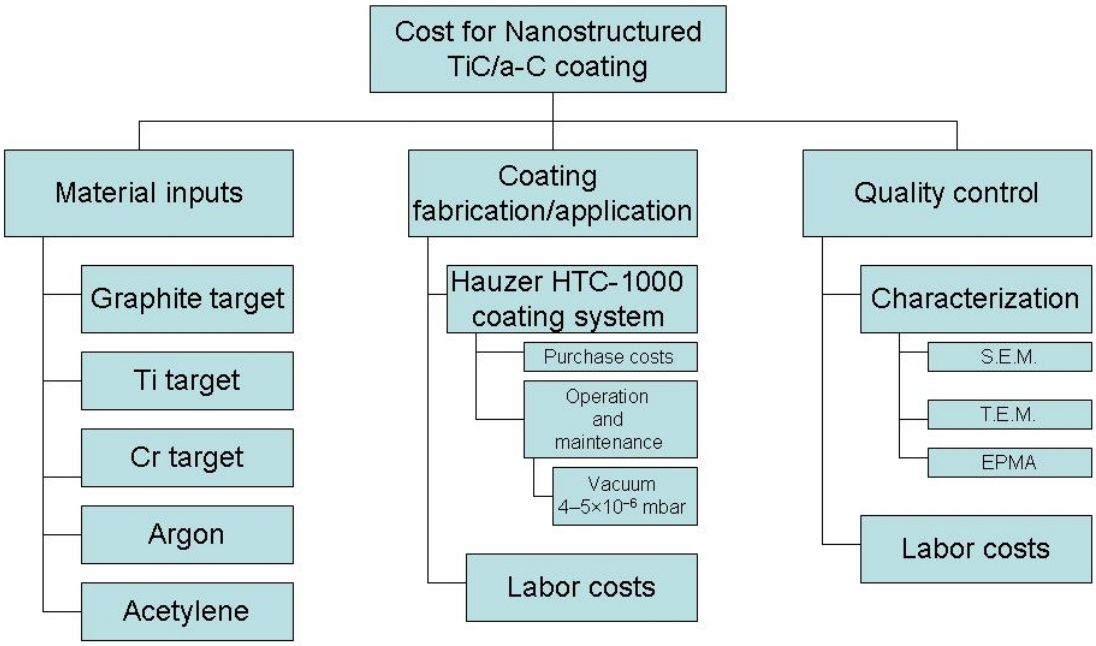

Figure 3.3: Cost structure of production of TiC/a-C coating.

Table 3.1: Estimated coating properties for TiC/a-C coating

Coating material	Coating thickness
TiC	5 μm (30% TiC by volume)
C	5 μm (70% C by volume)
Cr	1 μm

3.1.2 Thermal sprayed WC-Co coating

Thermal sprayed coatings have a significantly different cost structure and development process compared with coatings made with a physical vapor deposition method such as TiC/a-C discussed previously. Thermal spraying has been used for industrial coatings for decades and is a reasonably matured field. The use of thermal sprayed coatings for wear resistance was discussed in section 2.4.1.1, and some of the anti-corrosion coatings in section 2.4.1.4 are also applied through thermal spray processes. Thermal sprayed nanostructured WC-Co coatings have been discussed in multiple publications [53][54][150][151][152]. While there are many thermal spray methods which can be used to apply WC-Co coating, high velocity oxygen fuel (HVOF) is perhaps the most commonly used. In this method a fuel is mixed with oxygen and ignited in a combustion chamber. The combustion gases are then ejected at high speed towards the surface which will be coated and the coating material, in the form of a powder, is injected into the hot gas stream. The high temperature causes the powder to partially melt and is then deposited onto the surface of the substrate. In the case of the coating described by Kear et al. [151] the fuel used in the HVOF process was propane. The basic cost structure and

Table 3.2: Target costs for TiC/a-C coating

Target material	**Target size**	**Target cost** [149]	**Price per m^2 of coating**
Ti	12,56 in^2 x 0,125 in	€52	€2,6
C	12,56 in^2 x 0,125 in	€193	€28
Cr	12,56 in^2 x 0,125 in	€93	€0,36
Total cost per m^2 of coating		€32	

production process is outlined in Figure 3.4.

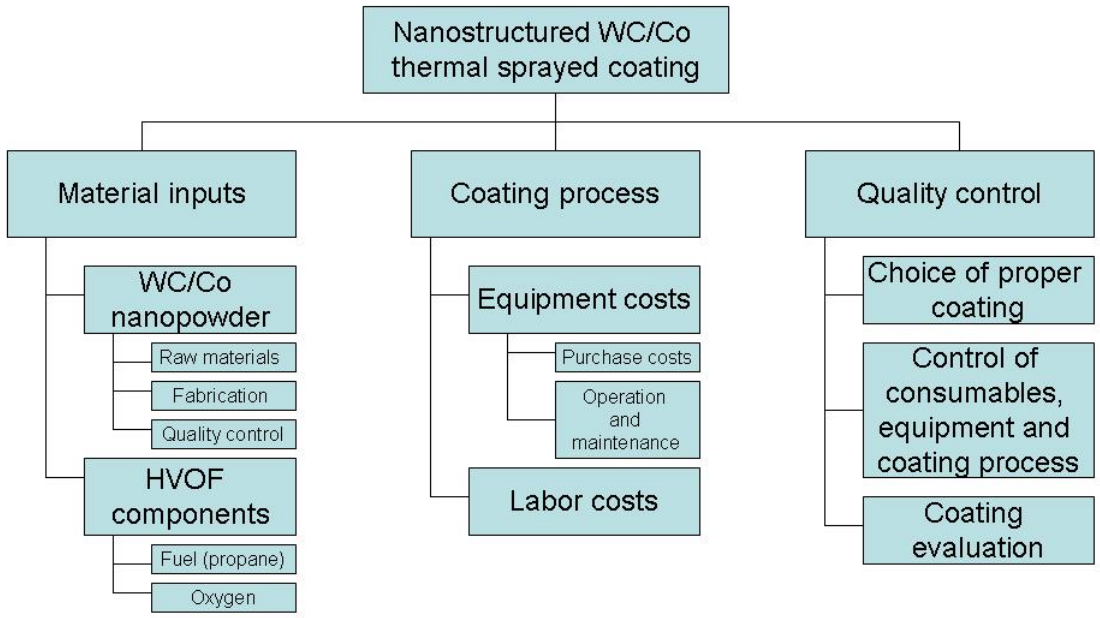

Figure 3.4: Cost structure of production of WC-Co thermal sprayed coating. Quality control measures are taken from Streiff et al. [153].

The nano powder feedstock is likely the most costly component of the thermal sprayed coating. Inframat® Advanced Materials™ LLC advertises WC-Co powder of grain size 40-80 nm at a cost of $ 385,00 for 1 kg. Inframat claims that the coatings formed from nano powders have a comparable density to conventional thermal sprayed coatings. Lovelock reviewed published literature on thermal sprayed WC-Co coatings and reported an average coating density of 13,3 g/cm^3. Assuming a coating thickness of 250 μm the price per square meter of coating due to powder costs is shown in Table 3.3. Another company, CiperTech, advertises conventional WC-Co thermal spray powders of grain size 15-45 μm

[154]. This is included in the table for comparison. From this table it can be seen the nanopowder coatings are between five and ten times the cost of the conventional coating.

Table 3.3: Estimated WC-Co powder costs

Material	**Powder cost per kg**	**Coating thickness**	**Coating density**	**Total cost per m^2**
Nano WC-Co powder	€266	250 μm	13.3 g/cm^3	€883
Convential WC-Co powder	€28-55	250 μm	13.3 g/cm^3	€92-184

3.1.3 Thermal sprayed anti-corrosion coating

The Nanosteel Company offers nanostructured corrosion resistant coatings which can be applied with thermal spray processes as discussed in section 2.4.1.4. The company would not disclose prices for the various products it offers and the only indication of a potential price range is a interview given in 2002 by the founder of the company stating a target price of approximately €44-55/kg of the coating feedstock. The coating of interest for corrosion resistant applicants is SHS 7570 which has a density of 7.59 g/cm^3. The cost per square meter for feedstock of this coating is shown in Table 3.4 assuming a coating thickness of 200 μm and a price of €70/kg.

Table 3.4: Estimated WC-Co powder costs

Material	**Powder cost per kg**	**Coating thickness**	**Coating density**	**Total cost per m^2**
SHS 7570	€70	200 μm	7,59 g/cm^3	€104

3.1.4 Thermoelectrics

While there are no nanostructured thermoelectric units currently in commercial production there are conventional semiconductor based thermoelectrics which are widely available. Nuwayhid et al. [105] reported prices in 2004 of €0.7-14 per watt of theoretical electrical output for their study in the use of thermoelectrics with small scale wood burning stoves. Table 3.5 shows the prices of commercially available thermoelectric generator modules from Custom Thermoelectric [110]. Rowe et al. [155] estimated that 80% of the costs of thermoelectrical generating systems come from unit costs, hence unit costs can serve as an acceptable basis for the cost estimation of the system.

Bismuth antimony telluride (BiSbTe) has been studied as a nanocomposite thermoelectric material [156][157]. As mentioned in section 2.4.4.1 nanocomposites are generally

Table 3.5: Commercially available thermoelectric module prices

Module number	Maximum theoretical output (W)	Price (€)	Price per watt (€/W)
1261G-7L31-04CQ	5,1	36	7,1
1261G-7L31-05CQ	7,15	36	5,1
1261G-7L31-10CX1	14,7	75	5,1

seen as having better scale up production potential than superlattices, and are of interest for potentially offering commercially viable thermoelectrics. The general method for production of the nanocomposites is by fabricating nanoparticles of the desired material which are then hot pressed to form the composite. BiSbTe nanocomposites have been produced which have maximum ZT values of 1,5 at room temperature [157] and 1,4 at 100 °C [156].

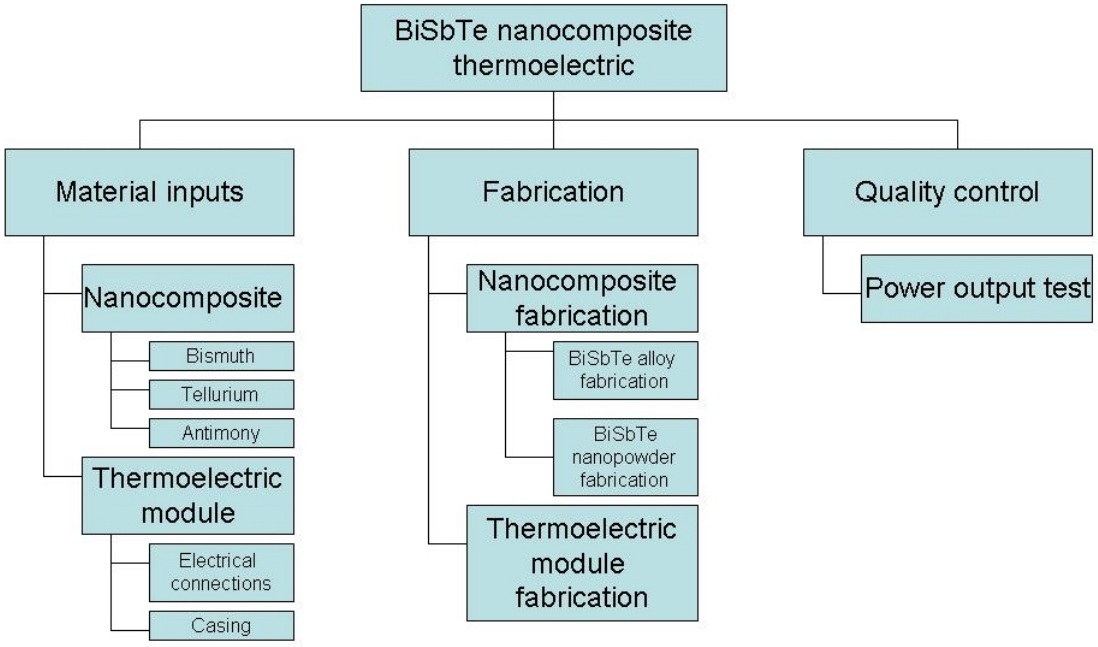

Figure 3.5: Cost structure of production of BiSbTe nanocomposite thermoelectrics.

3.2 Operational economic analysis

While section 3.1 discussed a framework for estimating the costs of nanotechnologies, it remains that determining an accurate estimate of the final product cost can be difficult. Companies also are often reluctant to discuss purchase costs and typical service costs for conventional equipment used in the bioenergy industry. Together, this can cause a direct economic comparison of conventional and nanotechnology solutions to be complicated. In this section the operational economics of selected nanotechnology solutions will be examined and estimates will be made where possible.

3.2.1 Wear resistant coatings

One of the primary areas of interest for wear resistant coatings are conveyor systems. For conveyor and handling systems the operational costs tend to be divided into three categories: energy; repairs and maintenance; and labor. Wear resistant coatings could offer potential cost reductions in the repairs and maintenance. There is little published information on the factors that influence the repair and maintenance costs of a conveyor systems and these costs tend to be given as a percentage of the initial capital investment which is expected to be spent per year. For some systems these costs can reach 20% per year. [158]

While there is no available information on the performance of nanocoatings in conveyor systems, some estimates can be made based on the wear performance in the published literature. Zirconia (ZrO_2) and WC-Co nanoparticles have both been used for improving wear resistance of coatings and tested under forces of 20-80 N. Wear rates were between 1/6 and 1/2 compared with the conventional powders. It was seen in section 3.1.2 that WC-Co nanopowder can cost between five and ten times the price of micron sized WC-Co powders. ZrO_2 nanopowders of size 30-60 nm can be purchased for approximately 3 times the cost of ZrO_2 of average size 0,3-0,7 mm in quantities of 1 kg [159].

If the initial investment and the maintenance and repair costs are the only two cost factors which change when replacing a component with a nanocoated part, the operational time required to payback the increased capital cost can be give by equation 3.1,

$$C_a + O_a T = C_b + O_b T, \tag{3.1}$$

where C_a is the capital cost of the convential component, O_a the operational cost of the convential component, C_b the capital cost of the nanocoated component, O_b the operational cost of the nanocoated component and T is years. As the operational costs are in this case entirely repair and maintenance costs which are given as a percentage of the capital costs, O_a can be written as M_aC_a, where M_a would be the repair and maintenance cost factor. Similarly O_b would be M_bC_b. It can be useful to write equation 3.1 in terms of C_b/C_a and M_b/M_a, and solving for T gives,

$$\frac{\frac{C_b}{C_a} - 1}{M_a(1 - \frac{M_b}{M_a})} = T. \tag{3.2}$$

If discounting is wished to be used to discount the future maintenance expenses to the present value then T can be replaced with the uniform series present worth factor,

$$\frac{(1+i)^n - 1}{i(1+i)^n}, \tag{3.3}$$

where i is the discount rate and n is the years. Solving for n gives,

$$n = \frac{ln(\frac{M_a(\frac{M_b}{M_a}-1)}{M_a(\frac{M_b}{M_a}-1)+(\frac{C_b}{C_a}-1)i})}{ln(1+i)}. \tag{3.4}$$

Equation 3.4 allows for the calculation of the discounted payback time given the ratio of capital costs of the two components, the maintenance cost of the original component as a percentage of the initial capital cost, and the ratio of the maintenance costs of the two components.

While these values are not available for currently used equipment such as conveyor systems or steel wear plates, some estimates can be used to show the process. Using the information for WC-Co nanoparticles compared with conventional WC-Co coatings discussed in section 3.1.2 the ratio C_b/C_a could be between five and ten. As discussed in section 2.4.1.1 the nanostructured coatings were shown to have a wear resistance of 1/6 to 1/2 of the conventional coating, and so M_b/M_a could be estimated to be between 1/6 and 1/2. If the maintenance cost for the original component was 20% of the initial capital cost per year then the time required to payback increased capital cost is shown in Figure 3.6. It is clear from this figure that if the replacement nanostructured components cost more than twice the conventional component, use of the nanostructured component would be hard to justify as the payback time grows to over ten years in most cases. In the case of maintenance costs being reduced to 1/6 of the original costs the payback time remains approximately eight years. If the price can be lowered to 1,5 times the conventional component the payback time becomes less than seven years and closer to four in the case of the largest reduction in maintenance costs. However, no nanotechnologies examined in this study offer solutions at this low of a price increase.

Heath and Skora [160] discussed the potential saving associated with wear resistant hardcoatings for hammermill grinding hammers. In their comparison noncoated, hardened steel hammers were compared with hammers coated with conventional hardfacing coatings but the same method can be used for analyzing the benefit of nanocoatings. Heath and Skora gave equation 3.5 in order to calculate the annual cost saving of surface coating a component rather than replacing it with a new part,

$$Annual\ cost\ savings = Yearly\ prod.\ rate * \frac{PC_N}{OP_N} * \frac{PC_R}{OP_R}, \tag{3.5}$$

where PC_N is the cost of the new part, OP_N is the cost of the hardfacing repair, OP_N is the work output during the life of the new part and OP_R is the work output during the life of the repaired part. In the example given by Heath and Skora it is claimed an uncoated cast hammer could cost €95 and last for one month while a coated hammer could cost €200 and last for five months. In this case not only would €275 be saved in purchase costs per hammer over 5 months by using the coated hammers but labor costs would also be decreased as the hammers need to be replaced less often. While the

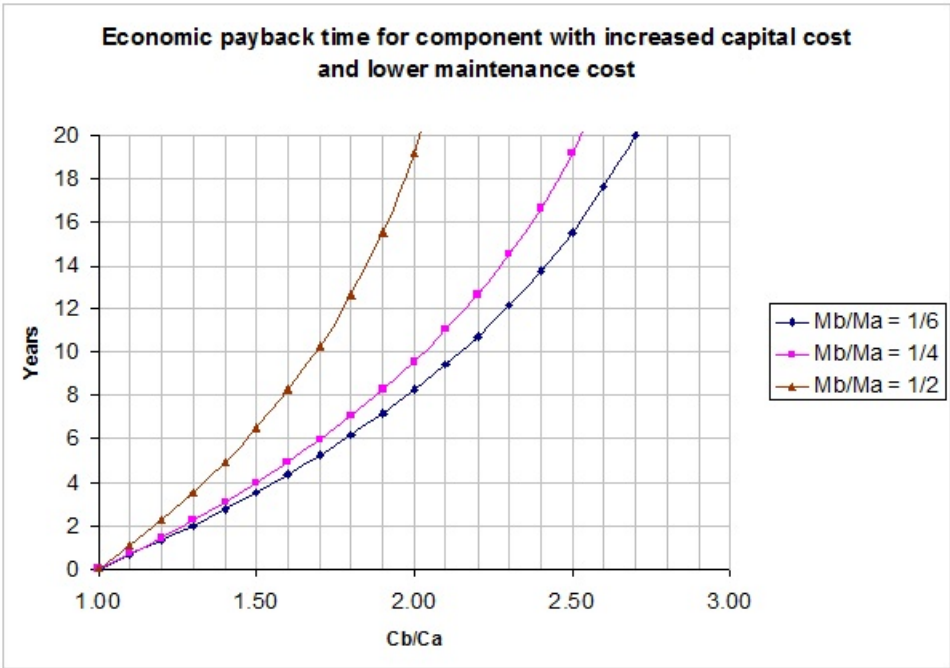

Figure 3.6: Economic payback time of a component with a higher initial capital cost and lower maintenance costs. Discount rate is 7,5% and the maintenance cost of the origional component is 20% of inital cost.

companies involved in processing of woody biomass in Finland were not able to provide specific figures on the life expectancy of the hammers currently in use, the values of one to five months nonetheless appear to be roughly accurate depending on the exact type of fuel being processed.

Nanostructured WC coatings and conventional WC coatings can be compared in a similar way. It was shown in section 3.1.2 that WC-Co nanopowders cost as much as ten times that of conventional WC-Co powders. If nanostructured WC-Co coated hammers have a similar order of magnitude cost increase as the powders then the hammers would need to last years to recover the cost. While WC-Co has been shown to have reduced wear rates under loads of 20-80 N and also increased hardness, Jia et al. [77] reported nanostructured WC-Co coatings do not necessarily have higher toughness than conventional WC-Co. This makes it difficult to estimate a performance life for nanocoated hammers without actual testing. It is clear though that nanostructured wear coatings are unlikely at this stage to last ten times longer than conventional coatings.

3.2.2 Corrosion resistance

The costs due to corrosion in biomass power plants have not been widely published. For fossil fuel power plants in the United States the cost due to corrosion was studied in a series of reports funded by the U.S. government. A report published in 2001 [161] found the total cost to the electricity generation industry due to corrosion in fossil fuel

power plants was €1.3 billion. There was a generation capacity of 488 GW and a total 2,227 million GWh of electricity generated during the same time. This gives an average of €2 700/GW of generation capacity per year or €580/GWh of generated electricity spent on corrosion related problems. While there are no studies available that would give a comparable cost for biomass power plants in Finland, these published values can be used as a starting point. If a corrosion protection coating such as the SHS 7570 produced by the NanoSteel Company reduces corrosion rates by 1/2 over the current method, it can be estimated that this would save approximately €300/GWh of electricity produced at the plant.

3.2.3 Thermoelectrics

An analysis of the economics of the operation of a thermoelectric generation system was performed by examining the discounted payback period in a variety of scenarios. As mentioned in section 3.1.4 the unit cost of a thermoelectric generation system has been estimated to be 80% of the total cost. As no published information was available about the remaining costs (maintenance, installation, etc.) they have been ignored for the time being. Figure 3.7 shows the economic payback time of thermoelectric units as a function of the unit price per watt and with five different discount rates. This calculation was done using the average 2010 electricity market price in Finland of €0,057/kWh [162]. As this scenario was intended to examine the feasibility of utilizing waste heat from a power plant, and an operational time of 8000 hours/year was used. The units listed in section 3.1.4 produced by Custom Thermoelectric had costs of approximately €5 and €7 per watt, corresponding to a payback time of 11 and 15 years respectively in the undiscounted calculation. In the 5% discount rate scenario the payback time increases to 16 and 30 years for the €5 and €7 per watt modules respectively. These calculations were repeated using an electricity price of double the 2010 market price, €0,11/kWh with the results shown in Figure 3.8. Figure 3.9 shows a similar scenario but in this case the discount rate remains constant at 7,5% for all the cases while the electricity prices range from €0,05/kWh to €0,175/kWh.

The economic payback time of a household thermoelectric system was also considered. In this scenario the electricity price was taken to be the 2010 average electricity price paid by consumers, €0,1235/kWh and the operational time was reduced to 3000 hours/year to represent a wood burning fireplace in a single family house. The results of these calculations are shown in Figure 3.10, where it can be seen that the payback times are longer in this case than the previous scenarios. For the undiscounted calculation the payback time was approximately 5,5 years when the module cost is €2/W, and at the current prices of €7/W the payback time is nearly 19 years.

Rowe [99] examined the electricity production cost over the lifetime of a 100 W thermoelectric generation system assuming varying construction costs. The thermoelectric

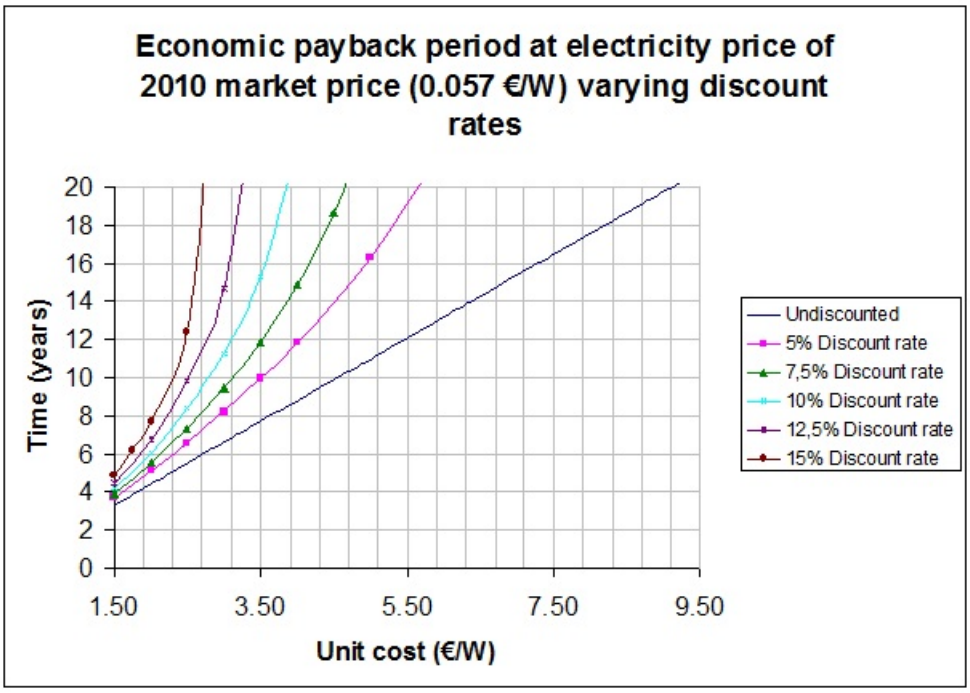

Figure 3.7: Economic payback time of thermoelectric units based on 2010 average market price of electricity in Finland.

system studied was developed under the Waste-heat Alternative Thermoelectric Technology (WATT) program. The results of this are shown in Figure 3.11 where it can be seen at the then current electricity costs of £0,08 per kWh the economic paypack time varied from approximately two years to more than twenty. The actual unit costs for the thermoelectric systems were not given in the study. This analysis was repeated for unit costs of €1,4-7,0/W and the 2010 average electricity price in Finland with the results shown in Figure 3.12. Using these input values the economic payback period ranges from approximately 4 to 14 years.

While research into thermoelectric materials has been ongoing for decades, widespread use of thermoelectric systems for electricity generation remains uncommon. This has resulted in relatively little information available on the operational life expectancy of the systems. However, thermoelectric generation systems have been used extensively in space applications over the past 50 years. From 1961 until 1990 there were a reported 22 U.S. spacecrafts launched which used thermoelectric generators to produce anywhere from 2,7 W to over 500 W [163]. The general operational parameter required for these space based applications was a service life of 15-20 years [164]. The Voyager 1 spacecraft was launched in 1977 with a thermoelectric generation system which produced about 470 W. In 2011 that system produces 270 W. Much of the drop in output power can be attributed to the decrease in power from the plutonium heat source. Taking into account the decay rate of the plutonium the thermoelectric materials can be estimated to have lost approximately

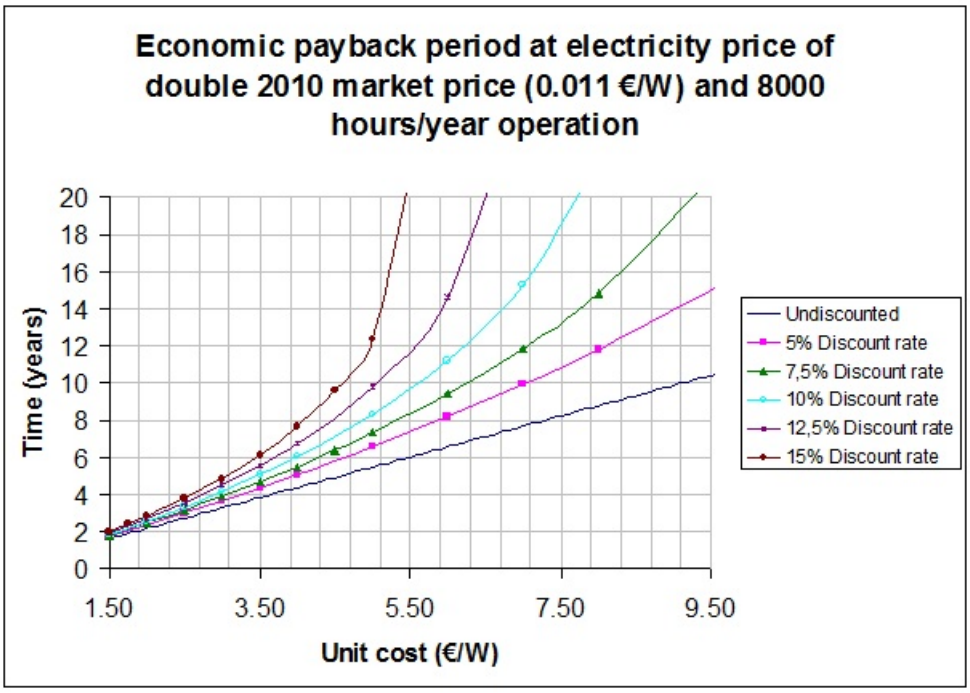

Figure 3.8: Economic payback time of thermoelectric units based on electricity price at double 2010 average market rate in Finland.

20% of their efficiency over 34 years. [165]

3.2.4 Screw conveyor low friction coating

Screw conveyors which feed fuel into the combustion chamber must be running at all times while the power plant is operational. This leads to an opportunity for cost saving by improving the performance of these conveyors. Owen and Cleary [166][167] have reported that particle-boundary friction in screw conveyors is a major factor in the power consumption of the conveyors. An "almost linear relationship between particle-boundary friction and the resulting power draw" of a screw conveyor is observed in one study [167]. This relationship was observed over the range of particle-boundary friction coefficients from 0,4 to 0,6. Nanosctructured low friction coatings such as those discussed in section 2.4.1.2, may have much lower frictional coefficient values and there is no available literature to show how far the linear relationship between frictional coefficient and power consumption may extend. A screw conveyor powered by a 1 kW electric motor could have an annual electricity cost of approximately €500 if run continuously. If the 20% decrease in power consumption observed by Owen and Cleary by reducing the particle-boundary coefficient of friction could be obtained this would represent an annual savings of approximately €100.

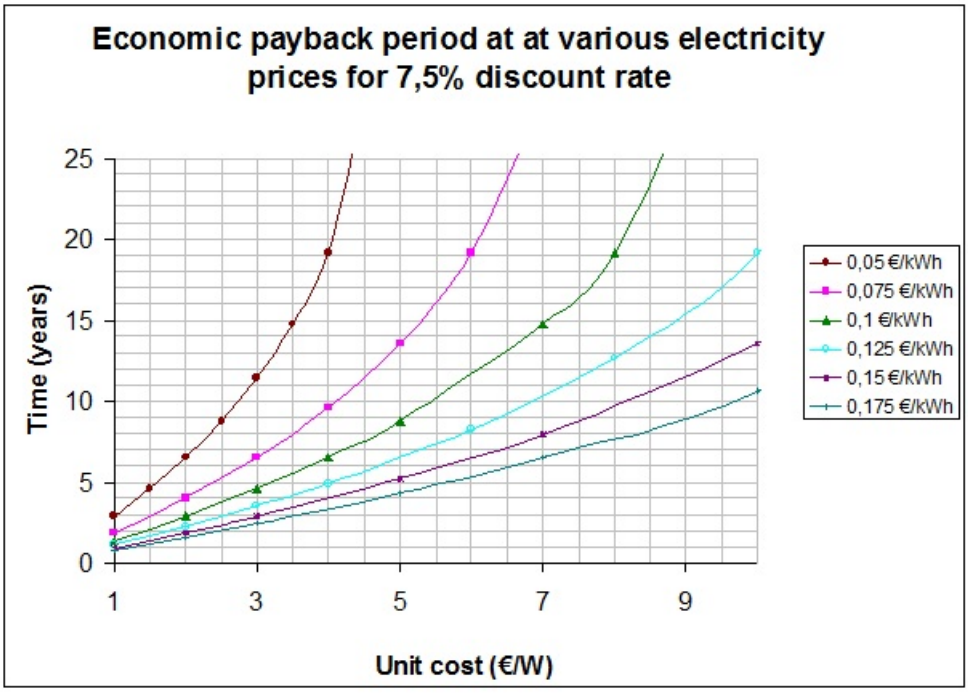

Figure 3.9: Economic payback time of thermoelectric units using discount rate of 7,5%.

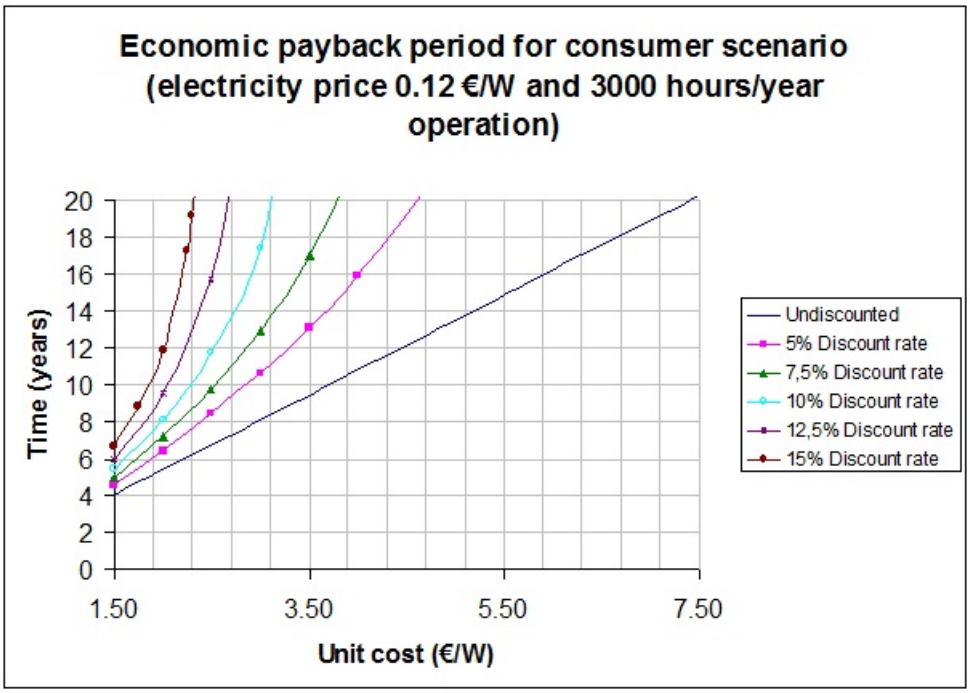

Figure 3.10: Economic payback time of thermoelectric units for a single house fireplace scenario at 2010 average consumer electricity prices.

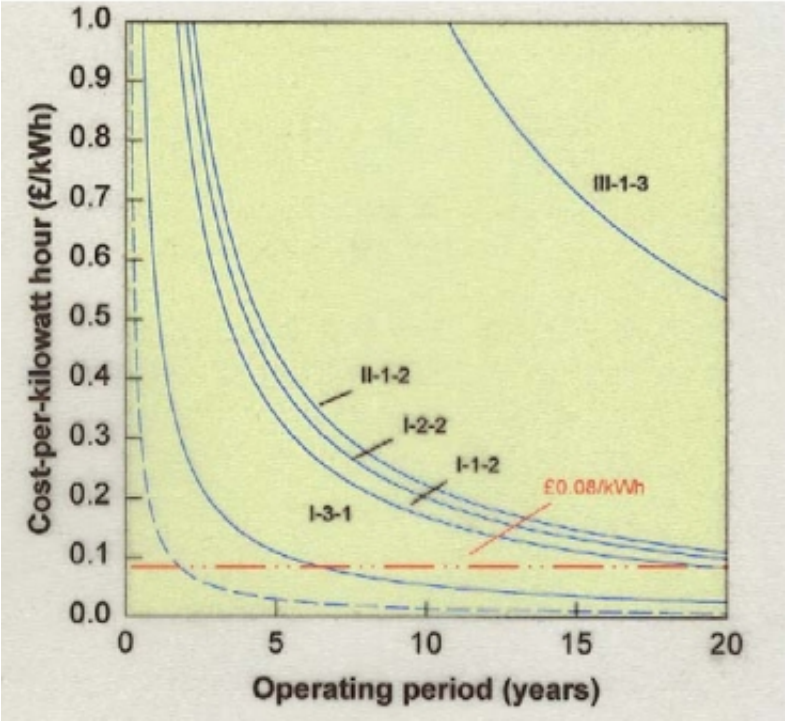

Figure 3.11: Electicity production costs of thermoelectric generation modules of varying unit costs [99].

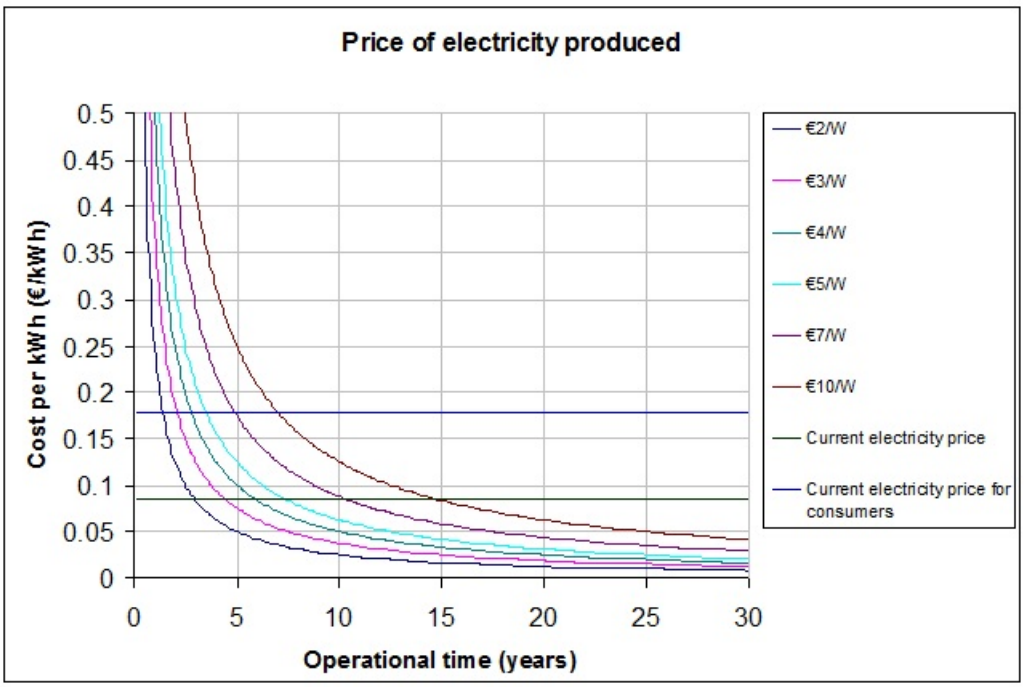

Figure 3.12: Electricity production costs of thermoelectric generation modules of varying production costs.

Chapter 4

Conclusions and recommendations for future work

This work has reviewed potential applications of nanotechnology in the production of electricity from biomass fuels and nanotechnology solutions to a set of problems of interest to the bioenergy industry in central Finland were examined. The current methods and technologies used in the bioenergy industry were discussed in Section 2.1, problems existing with those methods in Section 2.3, and nanotechnology solutions in Section 2.4. Chapter 3 discussed the economic viability of some of those nanotechnologies.

4.1 Conclusions

From these analyses a number of conclusions can be drawn:

- In general, nanotechnology offers a lot of potential in the bioenergy industry but the technologies tend to be either not yet developed enough for industrial use or not yet cost effective. The high costs of the nanotechnologies most often come from complicated production methods which have slow production rates.
- Wear resistant nanocoatings is an extremely large field with dozens of different materials currently being researched. Many coatings have significantly superior properties to conventional materials currently used in the bioenergy industry but the cost of the coatings limit their use to applications such as cutting tools.
- Low friction coatings need expensive deposition methods and their life expectancy under the conditions of a biomass fuel handling system is unknown. Use of these coatings in the short term will not be economically justifiable. However, use of low friction coatings on critical components such as screw conveyors is likely when production costs decrease.

- There are multiple potential coatings for corrosion protection in boilers but they are all either untested in high chlorine conditions of a biomass boiler or the performance results are unpublished. If tests show the already developed coatings work in biomass boiler conditions usage could begin quickly.

- Despite significant progress in recent years, set backs in the last year seem to have delayed the possibility of commercial anti-icing coatings. Even once anti-icing coatings with good performance are found it will take years to for them be a cost effective solution for the bioenergy industry.

- Nanomembranes have the possibility of allowing CO2 separation in flue gases, but the current state of this technology will become clearer when the NanoGLOWA project results are reported later in 2011.

- Thermoelectric materials have already been shown to be able to produce electricity from waste heat of power plants. At current costs of around €8/W the payback period would be over 15 years. Target costs for economically feasible thermoelectric systems for waste energy recovery in biomass power plants could be €1,5-2,5/W, which would give payback periods of 3-6 years. High efficiency nanostructured materials provide a good possibility for significantly reducing the cost per watt over the next decade.

- Thermophotovoltaics offer a potential method for CHP generation. Currently application is limited to small, household sized furnaces but costs must come down significantly for these to be economically viable. There are no industrial or commercial sized thermophotovoltaic systems in operation and development of any such system is most likely many years away.

4.2 Recommendations for future work

The following recommendations are made for continuing research into nanotechnology applications in bioenergy production:

- Nanotechnology is a rapidly changing field as new technologies emerge and current technologies are able to be produced at lower costs. This means that new publications should be reviewed for relevant technologies and economic analysis should be reevaluated to account for cost reductions if a significant amount of time has passed since the last review.

- Investigation into causes of peat adhesion to silo walls is needed, as the exact mechanisms for causing the adhesion are not currently well understood. Once the mechanisms causing the peat adhesion are better understood, determining if there are nanotechnology solutions will become easier.

- Further investigation into the results of the Nanomembranes against Global Warming (NanoGLOWA) project is recommended. The results of the project are scheduled to be released sometime in 2011, but are unavailable as of the time of writing.
- Testing of coatings which have been shown to provide corrosion protection for coal fire power plants in the chlorine environments of biomass boilers should be done. Coatings such as Cr_3C_2-25(Ni20Cr) [63], SHS 7570 [66], SHS 7170 [66], and the coating developed by VTT and Aalto University [87] appear to be the most promising.
- A more thorough analysis of the wear in the handling system is required for a better understanding of the costs associated with the use of wear resistant nanocoatings. Obtaining actual cost figures for current costs of these systems is essential in deciding if nanocoatings could be cost effective. Taking into account potential savings through use of lower cost steel when using a wear resistant coating rather than more expensive wear resistant steel which is currently used could provide more clear picture of the economic viability of the coatings.

Appendix A

Vicker's Hardness values

Vicker's hardness test is a commonly used technique to evaluate the hardness of a material. It is preformed by using an indenter on the test material and measuring the force applied to the indenter and the surface area of the impression left. The Vicker's hardness, H_v, is given by equation A.1,

$$H_v = \frac{1854,4 * P}{d^2}, \tag{A.1}$$

where P is the load and d is the diagonal of the square-based diamond pyramid indenter [168]. This value is usually reported with the units of kgf/mm^2, however they are often omitted when writing the value. In scientific works it has become common to report the value using SI units, either as kg/mm^2 or GPa. All values have been converted to GPa for Table 2.4. An example of the conversion is given for the NanoSteel Company coating SHS 7214. The value was originally reported as a value of 57 HR$_c$ using the Rockwell C Hardness scale, which was converted to a Vicker's hardness of 640 kgf/mm^2 using conversion tables [169]. Once in units of kgf/mm^2 the value was converted to GPa as shown in equation A.2

$$640\frac{kgf}{mm^2} = 640\frac{kgf}{mm^2} * 9,8\frac{N}{kgf} * 1/1000\frac{kN}{N} = 6,3\frac{kN}{mm^2} = 6,3GPa. \tag{A.2}$$

Appendix B

Titanium carbide/amorphous carbon coating cost estimation

In section 3.1.1 a cost estimation was made for the targets required to deposit a TiC/a-C coating using pulsed laser deposition. The assumptions used in the calculations were given in section 3.1.1, but the calculations will be shown in more detail. Assuming a density of 4,9 g/cm^3 for titanium carbide, a 5 μm thick layer of Ti would have a mass of 24,5 g/m^2, as shown by equation B.1,

$$Mass\,per\,m^2\,of\,coating = 4,9\frac{g}{cm^3} * 0.0001\frac{cm}{\mu m} * 5\mu m * 10000\frac{cm^2}{m^2} = 24,5g/m^2. \quad \text{(B.1)}$$

However, the TiC makes up only 30% of the matrix by volume, with the rest being composed of amorphous carbon. As a result the TiC in the 5 μm thick layer would have a mass of 7,35 g/m^2. From the molar mass of TiC 7,35 g/m^2 is equivalent to 0,12 moles/m^2. The size of the Ti target was 12,56 in^2 by 0,125 in which gives a volume of 2.57*10^{-5} m^3. Using the density of Ti, 4,5 g/cm^3, it can be calculated that the target contains approximately 2,4 moles of Ti atoms.

$$Cost\,of\,Ti\,target\,per\,m^2\,of\,coating = \frac{52\frac{e}{target}}{2,4\frac{moles}{target}} * 0.12\frac{moles}{m^2} = 2,6\frac{e}{m^2}. \quad \text{(B.2)}$$

This is the result which can be seen in Table 3.2 for the cost of the Ti target per m^2 of coating. The same process was repeated for carbon and chromium.

Appendix C

Discounted payback period

The payback period is defined as the time required for returns to equal the original expenditure. In the case of the thermoelectric generation systems described in section 3.2.3 the returns were assumed to be yearly cash flows equal to the total revenue generated by selling electricity at the 2010 average electricity rate of €0,057 per kWh for 8760 hours (365 days). The undiscounted payback period was calculated using Equation C.1,

$$Payback\ period = \frac{Unit\ cost\ per\ kilowatt}{8670\ hours * 0,057\ \frac{e}{kWh}}. \tag{C.1}$$

The discounted payback period was calculated by calculating the net present value of the cash flows for each year, assuming the discount rate shown in Figure 3.7. Calculating the discounted net present value (DNPV) series of cash flows can be done using Equation C.2,

$$P = \sum_{t=0}^{N} \frac{R_t}{(1+i)^t}, \tag{C.2}$$

where P is the discounted net present value, t is the year, R_t is the revenue of year t valued in year t, i is the discount rate and N is the final year of revenue. If R_t is constant then this summation can be written in terms of the uniform series present worth factor,

$$P = R[\frac{(1+i)^n - 1}{i(1+i)^n}], \tag{C.3}$$

where R is the constant R_t from equation C.2. Solving this for the year, n, gives

$$n = \frac{ln - (\frac{R}{iP-R})}{ln(i+1)}. \tag{C.4}$$

As an example, using a discount rate of 7.5%, a module cost of €2/W, a module size of 1 kW, an electricity price of €0,057/kWh and 8000 hours per year of operation the payback period would be:

$$n = \frac{ln(\frac{456}{0,075*2000-456})}{ln(0,075+1)} = 3,9. \tag{C.5}$$

This shows that given these conditions it would take 3,9 years to earn back the initial investment.

References

[1] Statistics Finland. Energy consumption 2009, 2010. URL http://www.stat.fi/til/ekul/2009/ekul_2009_2010-12-10_en.pdf.

[2] U.S. Energy Information Administration. Annual energy review, 2009. URL http://www.eia.doe.gov/emeu/aer/overview.html.

[3] M. Roco. International perspective on government nanotechnology funding in 2005. *Journal of Nanoparticle Research*, 7:707–712, 2005. URL http://dx.doi.org/10.1007/s11051-005-3141-5.

[4] Mechael Grieneisen. The proliferation of nano journals. *Nature Nanotechnology*, 5, 2010. URL http://dx.doi.org/10.1038/nnano.2010.216.

[5] Can Huang, Ad Notten, and Nico Rasters. Nanoscience and technology publications and patents: a review of social science studies and search strategies. *The Journal of Technology Transfer*, 36: 145–172, 2011. URL http://dx.doi.org/10.1007/s10961-009-9149-8.

[6] Recycling Today. Norco equipment introduces horizontal grinder, 2010. URL http://www.recyclingtoday.com/norco-dynamic-5240.aspx.

[7] University of Tennessee Biosystems Engineering & Soil Science. Bioprocessing bess utk, 2006. URL http://www.biomassprocessing.org/grinding_sizereduction_actionspage.htm.

[8] Sjaak Van Loo and Japp Koppejan, editors. *The Handbook of Biomass Combustion and Co-firing*. Earthscan, 2008.

[9] Thomas F. McGowan, Micheal L. Brown, William S. Bulpitt, and James L. Walsh Jr., editors. *Biomass and Alternate Fuel Systems: An Engineering and Economic Guide*. Wiley-AIChE, 2009.

[10] V R. Undeger, V. Cariapa, T H. Wenzel, and B. Moussa. Mechanical conveying - chain pull force characteristics when conveying cement clinker in a drag chain conveyor. *Bulk Solid Handling*, 21, 2001.

[11] Eija Alakangas. Bioenergy in finland: Review 1998. Technical report, VTT, 1998. URL http://www.finbioenergy.fi/bioenergy_in_finland/5_2fuel_hand.htm.

[12] Timo Jarvinen. The analysis report of plant no. 1: Cofiring of biomass - evaluation of fuel procurement and handling in selected existing plants and exchange of information (cofiring) - part 2. Technical report, VTT, 2000.

[13] Wärtsilä. Biopower solutions, 2007. URL www.netequity.biz/docs/BioChip/WartsilaPP.pdf.

[14] IEA. Biomass for power generation and chp. URL http://www.iea.org/techno/essentials3.pdf.

[15] Larry Drbal, Kayla Westra, Pat Boston, and R. Bruce Erikson, editors. *Power Plant Engineering*. 1995.

[16] URL http://www.fwc.com/publications/GPGPressReleases/release080607.pdf.

[17] Angela Neville. Top Plant: Kaukaan Voima Oy Biomass-Fired Power Plant, Lappeenranta, Finland.

[18] Richard van den Broek, André Faaij, and Ad van Wijk. Biomass combustion for power generation. *Biomass and Bioenergy*, 11(4):271 – 281, 1996. URL http://dx.doi.org/10.1016/0961-9534(96)00033-5.

[19] Larry L. Baxter, Thomas R. Miles, Thomas R. Miles, Bryan M. Jenkins, Thomas Milne, David Dayton, Richard W. Bryers, and Larry L. Oden. The behavior of inorganic material in biomass-fired power boilers: field and laboratory experiences. *Fuel Processing Technology*, 54(1-3):47 – 78, 1998. URL http://dx.doi.org/10.1016/S0378-3820(97)00060-X.

[20] Xiaolin Wei, Uwe Schnell, and Klaus R.G. Hein. Behaviour of gaseous chlorine and alkali metals during biomass thermal utilisation. *Fuel*, 84(7-8):841 – 848, 2005. URL http://dx.doi.org/10.1016/j.fuel.2004.11.022.

[21] Matti Hiltunen, Vesna Barišić, and Edgardo Coda Zabetta. Combustion of different types of biomass in CFB boilers. In *16th European Biomass Conference*, 2008.

[22] H. P. Nielsen, L. L. Baxter, G. Sclippab, C. Morey, F. J. Frandsen, and K. Dam-Johansen. Deposition of potassium salts on heat transfer surfaces in straw-fired boilers: a pilot-scale study. *Fuel*, 79(2):131 – 139, 2000. URL http://dx.doi.org/10.1016/S0016-2361(99)00090-3.

[23] H. P. Nielsen, F. J. Frandsen, K. Dam-Johansen, and L. L. Baxter. The implications of chlorine-associated corrosion on the operation of biomass-fired boilers. *Progress in Energy and Combustion Science*, 26(3):283 – 298, 2000. URL http://dx.doi.org/10.1016/S0360-1285(00)00003-4.

[24] Hadj Latreche. *Development of protective coatings to improve high temperature corrosion resistance in chlorine containing environments based on an advanced corrosion risk assessment tool.* PhD thesis, RWTH Aachen University, 2009.

[25] H. Worch and P. Kofstad. High temperature corrosion. *Crystal Research and Technology*, 24(4):378–378, 1989. URL http://dx.doi.org/10.1002/crat.2170240408.

[26] Robert Winston Revie and Herbert Henry Uhlig, editors. *Corrosion and corrosion control; an introduction to corrosion science and engineering.* Wiley-Interscience, 2008.

[27] D. Gandy. Program on technology innovation: State of knowledge review of nanostructure coatings for boiler tube application. Technical report, Electric Power Research Institute, 2007.

[28] M. A. Uusitalo, P. M. J. Vuoristo, and T. A. Mäntylä. High temperature corrosion of coatings and boiler steels in oxidizing chlorine-containing atmosphere. *Materials Science and Engineering A*, 346(1-2):168 – 177, 2003. URL http://dx.doi.org/10.1016/S0921-5093(02)00537-3.

[29] R. Bender and M. Schütze. The role of alloying elements in commercial alloys for corrosion resistance in oxidizing-chloridizing atmospheres. part i: Literature evaluation and thermodynamic calculations on phase stabilities. *Materials and Corrosion*, 54(8):567–586, 2003. URL http://dx.doi.org/10.1002/maco.200390129.

[30] M. A. Uusitalo, P. M. J. Vuoristo, and T. A. Mäntylä. High temperature corrosion of coatings and boiler steels below chlorine-containing salt deposits. *Corrosion Science*, 46(6):1311 – 1331, 2004. URL http://dx.doi.org/10.1016/j.corsci.2003.09.026.

[31] B.-J. Skrifvars, R. Backman, M. Hupa, K. Salmenoja, and E. Vakkilainen. Corrosion of superheater steel materials under alkali salt deposits part 1: The effect of salt deposit composition and temperature. *Corrosion Science*, 50(5):1274 – 1282, 2008. URL http://dx.doi.org/10.1016/j.corsci.2008.01.010.

[32] Martti Aho. Reduction of chlorine deposition in FB boilers with aluminium-containing additives. *Fuel*, 80(13):1943 – 1951, 2001. URL http://dx.doi.org/10.1016/S0016-2361(01)00049-7.

[33] Bu-Qian Wang. Erosion-corrosion of coatings by biomass-fired boiler fly ash. *Wear*, 188(1-2):40 – 48, 1995. URL http://dx.doi.org/10.1016/0043-1648(95)06598-9.

[34] A.A. Khan, W. de Jong, P.J. Jansens, and H. Spliethoff. Biomass combustion in fluidized bed boilers: Potential problems and remedies. *Fuel Processing Technology*, 90(1):21 – 50, 2009. URL http://dx.doi.org/10.1016/j.fuproc.2008.07.012.

[35] Buta Sidhu and S. Prakash. Nickel-chromium plasma spray coatings: A way to enhance degradation resistance of boiler tube steels in boiler environment. *Journal of Thermal Spray Technology*, 15: 131–140, 2006. URL http://dx.doi.org/10.1361/105996306X92695. 10.1361/105996306X92695.

[36] Klaus Erich Schneider, Vladimir Belaschenko, Marian Dratwinski, Stephan Siegmann, and Alexander Zagorski, editors. *Thermal Spraying for Power Generation Components*. 2006.

[37] S. Tuurna, T. Varis, K. Penttilä, K. Ruusuvuori, S. Holmström, and S. Yli-Olli. Optimised selection of new protective coatings for biofuel boiler applications. *Materials and Corrosion*, 2010. doi: DOI:10.1002/maco.201005898. URL http://dx.doi.org/10.1002/maco.201005898.

[38] P. Butschbach, F. Hammer, H. Kohler, A. Potreck, and T. Trautmann. Extensive reduction of toxic gas emissions of firewood-fueled low power fireplaces by improved in situ gas sensorics and catalytic treatment of exhaust gas. *Sensors and Actuators B: Chemical*, 137(1):32 – 41, 2009. URL http://dx.doi.org/10.1016/j.snb.2008.12.007.

[39] VTT. Biomass CHP - finland. URL http://www.cres.gr/biocogen/pdf/events/Biomass%2520CHP%2520-%2520Finland%2520Ateena.pdf.

[40] Marc A. Rosen, Minh N. Le, and Ibrahim Dincer. Efficiency analysis of a cogeneration and district energy system. *Applied Thermal Engineering*, 25(1):147 – 159, 2005. URL http://dx.doi.org/10.1016/j.applthermaleng.2004.05.008.

[41] Fibrocom. New generation of containers. Online. URL http://www.fibrocom.com/index.php?page=containers&container=eng.

[42] Mauri Laitinen. Thinking beyond honeycomb structures. Online, 2006. URL http://www.hightech.fi/direct.aspx?area=htf&prm1=137&prm2=article.

[43] Genesis III Inc. Genesis iii - superior hammermill components, 2006. URL http://www.g3hammers.com/hammers.php.

[44] James S. Rhodes and David W. Keith. Engineering economic analysis of biomass IGCC with carbon capture and storage. *Biomass and Bioenergy*, 29(6):440 – 450, 2005. URL http://dx.doi.org/10.1016/j.biombioe.2005.06.007.

[45] Yuanjing Zheng, Anker Degn Jensen, and Jan Erik Johnsson. Deactivation of V_2O_5-WO_3-TiO_2 SCR catalyst at a biomass-fired combined heat and power plant. *Applied Catalysis B: Environmental*, 60(3-4):253 – 264, 2005. URL http://dx.doi.org/10.1016/j.apcatb.2005.03.010.

[46] Ann-Charlotte Larsson, Jessica Einvall, Arne Andersson, and Mehri Sanati. Targeting by comparison with laboratory experiments the SCR catalyst deactivation process by potassium and zinc salts in a large-scale biomass combustion boiler. *Energy & Fuels*, 20(4):1398–1405, 2006. URL http://dx.doi.org/10.1021/ef060077u.

[47] Joshua R. Strege, Christopher J. Zygarlicke, Bruce C. Folkedahl, and Donald P. McCollor. SCR deactivation in a full-scale cofired utility boiler. *Fuel*, 87(7):1341 – 1347, 2008. URL http://dx.doi.org/10.1016/j.fuel.2007.06.017.

[48] P. M. Ajayan, L. S. Schadles, and P. V. Braun, editors. *Nanocomposite Science and Technology*. Wiley-VCH, 2003.

[49] Vikas Chawla, Buta Singh Sidhu, D. Puri, and S. Prakash. State of art: Plasma sprayed nanostructured coatings: A review. *Materials Forum*, 32, 2008. URL http://dx.doi.org/10.1002/maco.200503899.

[50] You Wang, Stephen Jiang, Meidong Wang, Shihe Wang, T. Danny Xiao, and Peter R. Strutt. Abrasive wear characteristics of plasma sprayed nanostructured alumina/titania coatings. *Wear*, 237(2):176 – 185, 2000. URL http://dx.doi.org/10.1016/S0043-1648(99)00323-3.

[51] Huang Chen, Yefan Zhang, and Chuanxian Ding. Tribological properties of nanostructured zirconia coatings deposited by plasma spraying. *Wear*, 253(7-8):885 – 893, 2002. URL http://dx.doi.org/10.1016/S0043-1648(02)00221-1.

[52] D. Branagan, M. Breitsameter, B. Meacham, and V. Belashchenko. High-performance nanoscale composite coatings for boiler applications. *Journal of Thermal Spray Technology*, 14:196–204, 2005. URL http://dx.doi.org/10.1361/10599630523755. 10.1361/10599630523755.

[53] Ying chun Zhu, Ken Yukimura, Chuan xian Ding, and Ping yu Zhang. Tribological properties of nanostructured and conventional wc-co coatings deposited by plasma spraying. *Thin Solid Films*, 388(1-2):277 – 282, 2001. URL http://dx.doi.org/10.1016/S0040-6090(01)00805-7.

[54] D. A. Stewart, P. H. Shipway, and D. G. McCartney. Abrasive wear behaviour of conventional and nanocomposite HVOF-sprayed WC-Co coatings. *Wear*, 225-229(Part 2):789 – 798, 1999. URL http://dx.doi.org/10.1016/S0043-1648(99)00032-0.

[55] X.M. Meng, W.Z. Tang, L.F. Hei, C.M. Li, S.J. Askari, G.C. Chen, and F.X. Lu. Application of cvd nanocrystalline diamond films to cemented carbide drills. *International Journal of Refractory Metals and Hard Materials*, 26(5):485 – 490, 2008. URL http://dx.doi.org/10.1016/j.ijrmhm.2007.11.006.

[56] Yusheng Zhao, Jiang Qian, Luke L. Daemen, Cristian Pantea, Jianzhong Zhang, Georgiy A. Voronin, and T. Waldek Zerda. Enhancement of fracture toughness in nanostructured diamond–sic composites. *Applied Physics Letters*, 84(8):1356–1358, 2004. URL http://dx.doi.org/10.1063/1.1650556.

[57] Neil Canter. Bam: Antiwear and friction-reducing coating. *Tribology & Lubrication Technology*, March 2009.

[58] Wei Wang, Feng-Yan Hou, Hui Wang, and He-Tong Guo. Fabrication and characterization of Ni-ZrO_2 composite nano-coatings by pulse electrodeposition. *Scripta Materialia*, 53(5):613 – 618, 2005. URL http://dx.doi.org/10.1016/j.scriptamat.2005.04.002.

[59] Qiuyuan Feng, Tingju Li, Haitao Teng, Xiaoli Zhang, Yu Zhang, Changsheng Liu, and Junze Jin. Investigation on the corrosion and oxidation resistance of Ni-Al_2O_3 nano-composite coatings prepared by sediment co-deposition. *Surface and Coatings Technology*, 202(17):4137 – 4144, 2008. URL http://dx.doi.org/10.1016/j.surfcoat.2008.03.001.

[60] Suman Kumari Mishra. Nano and nanocomposite superhard coatings of silicon carbonitride and titanium diboride by magnetron sputtering. *International Journal of Applied Ceramic Technology*, 6(3):345–354, 2009. URL http://dx.doi.org/10.1111/j.1744-7402.2008.02287.x.

[61] G.K. Dosbaeva, S.C. Veldhuis, K. Yamamoto, D.S. Wilkinson, B.D. Beake, N. Jenkins, A. Elfizy, and G.S. Fox-Rabinovich. Oxide scales formation in nano-crystalline TiAlCrSiYN PVD coatings at elevated temperature. *International Journal of Refractory Metals and Hard Materials*, 28(1): 133 – 141, 2010. URL http://dx.doi.org/10.1016/j.ijrmhm.2009.09.003. Tribology of Hard Coatings.

[62] Jianhong He, Michael Ice, and Enrique Lavernia. Synthesis of nanostructured Cr_3C_2-25(Ni20Cr) coatings. *Metallurgical and Materials Transactions A*, 31:555–564, 2000. URL http://dx.doi.org/10.1007/s11661-000-0290-0. 10.1007/s11661-000-0290-0.

[63] A. Padial, C.A. Cunha, O.V. Correa, and L.V. Ramanathan. Thermal stability and erosion-oxidation behavior of nanostructured Cr_3C_2-Ni20Cr coating. In *19 Congresso Brasileiro de Engenharia e Ciência dos Materiais*, pages 6025–6031, 2010.

[64] T. Sundararajan, S. Kuroda, J. Kawakita, and S. Seal. High temperature corrosion of nanoceria coated 9Cr-1Mo ferritic steel in air and steam. *Surface and Coatings Technology*, 201(6):2124 – 2130, 2006. URL http://dx.doi.org/10.1016/j.surfcoat.2006.02.007.

[65] Zhenyu Liu, Wei Gao, and Meishuan Li. Cyclic oxidation of sputter-deposited nanocrystalline Fe-Cr-Ni-Al alloy coatings. *Oxidation of Metals*, 51:403–419, 1999. URL http://dx.doi.org/10.1023/A:1018835126181.

[66] The NanoSteel Company. Biomass boiler tube coatings. Online. URL http://www.nanosteelco.com/power/biomass_boiler_tube_coatings.html.

[67] Wei Gao and Zhengwei Li. Nano-structured alloy and composite coatings for high temperature applications. *Materials Research*, 7:175 – 182, 03 2004. URL http://dx.doi.org/10.1590/S1516-14392004000100023.

[68] Liangliang Cao, Andrew K. Jones, Vinod K. Sikka, Jianzhong Wu, and Di Gao. Anti-icing superhydrophobic coatings. *Langmuir*, 25(21):12444–12448, 2009. URL http://dx.doi.org/10.1021/la902882b. PMID: 19799464.

[69] S.A. Kulinich and M. Farzaneh. Ice adhesion on super-hydrophobic surfaces. *Applied Surface Science*, 255(18):8153 – 8157, 2009. URL http://dx.doi.org/10.1016/j.apsusc.2009.05.033.

[70] Vladimir Bata and Elena V. Pereloma. An alternative physical explanation of the hall-petch relation. *Acta Materialia*, 52(3):657 – 665, 2004. URL http://dx.doi.org/10.1016/j.actamat.2003.10.002.

[71] M. Zhao, J. C. Li, and Q. Jiang. Hall-petch relationship in nanometer size range. *Journal of Alloys and Compounds*, 361(1-2):160 – 164, 2003. ISSN 0925-8388. URL http://dx.doi.org/10.1016/S0925-8388(03)00415-8.

[72] D. Kalyanasundaram and P. Molian. Electrodeposition of nanodiamond particles on aluminium alloy a319 for improved tribological properties. *Micro Nano Letters, IET*, 3(4):110 –116, 2008. URL http://dx.doi.org/10.1049/mnl:20080023.

[73] B.H. Kear. Plasma-sprayed nanostructured al2o3/tio2 powders and coatings. *Journal of Thermal Spray Technology*, 9:483–487(5), 1 December 2000. URL http://dx.doi.org/10.1361/105996300770349683.

[74] Sam Zhang, Deen Sun, Yongqing Fu, and Hejun Du. Recent advances of superhard nanocomposite coatings: a review. *Surface and Coatings Technology*, 167(2-3):113 – 119, 2003. URL http://dx.doi.org/10.1016/S0257-8972(02)00903-9. Proceedings of the Symposium on Technological Advances and Performance of Engineering Thin Films and Surface Coatings at the 1st International Conference on Materials Processing for Properties and Performance (MP3).

[75] D. K. Shetty, I. G. Wright, P. N. Mincer, and A. H. Clauer. Indentation fracture of WC-Co cermets. *Journal of Materials Science*, 20:1873–1882, 1985. URL http://dx.doi.org/10.1007/BF00555296.

[76] Li Zhang, Yuan jie Wang, Xian wang Yu, Shu Chen, and Xiang jun Xiong. Crack propagation characteristic and toughness of functionally graded WC-Co cemented carbide. *International Journal of Refractory Metals and Hard Materials*, 26(4):295 – 300, 2008. URL http://dx.doi.org/10.1016/j.ijrmhm.2007.07.002.

[77] K. Jia, T. E. Fischer, and B. Gallois. Microstructure, hardness and toughness of nanostructured and conventional WC-Co composites. *Nanostructured Materials*, 10(5):875 – 891, 1998. URL http://dx.doi.org/10.1016/S0965-9773(98)00123-8. Selected Papers from the Conference on Microstructure and its Effects on Amorphous, Nanophase and Nanocrystalline Materials TMS Annual Meeting and Exposition.

[78] A. A. Voevodin and J. S. Zabinski. Supertough wear-resistant coatings with 'chameleon' surface adaptation. *Thin Solid Films*, 370(1-2):223 – 231, 2000. URL http://dx.doi.org/10.1016/S0040-6090(00)00917-2.

[79] S. Veprek and S. Reiprich. A concept for the design of novel superhard coatings. *Thin Solid Films*, 268(1-2):64 – 71, 1995. ISSN 0040-6090. URL http://dx.doi.org/10.1016/0040-6090(95)06695-0.

[80] K. Yamamoto, Hirotaka Ito, and S. Kujime. Nano-multilayered CrN/BCN coating for anti-wear and low friction applications. *Surface and Coatings Technology*, 201(9-11):5244 – 5248, 2007. URL http://dx.doi.org/10.1016/j.surfcoat.2006.07.165. Proceedings of the Fifth Asian-European International Conference on Plasma Surface Engineering - AEPSE 2005, Proceedings of the Fifth Asian-European International Conference on Plasma Surface Engineering.

[81] Y.Y. Liu, J. Yu, H. Huang, B.H. Xu, X.L. Liu, Y. Gao, and X.L. Dong. Synthesis and tribological behavior of electroless ni-p-wc nanocomposite coatings. *Surface and Coatings Technology*, 201 (16-17):7246 – 7251, 2007. URL http://dx.doi.org/10.1016/j.surfcoat.2007.01.035.

[82] Mohammod Aminuzzaman, Yuko Kado, Masaya Mitsuishi, and Tokuji Miyashita. Frictional properties of an immobilized fluorinated polymer nanosheet. *Thin Solid Films*, 516(1):67 – 71, 2007. URL http://dx.doi.org/10.1016/j.tsf.2007.05.025.

[83] Robert A. Feeler. De-icing and anti-icing are major safety factors in winter operations. *Aviation Mechanics Bulletin*, November/December 1991.

[84] S. A. Kulinich, S. Farhadi, K. Nose, and X. W. Du. Superhydrophobic surfaces: Are they really ice-repellent? *Langmuir*, 27(1):25–29, 2011. URL http://dx.doi.org/10.1021/la104277q.

[85] David N. Anderson and Allen D. Reich. Tests of the performance of coatings for low ice adheasion. In *35th Aerospace Sciences Meeting Exhibit*, 1997.

[86] Kripa K. Varanasi, Tao Deng, J. David Smith, Ming Hsu, and Nitin Bhate. Frost formation and ice adhesion on superhydrophobic surfaces. *Applied Physics Letters*, 97(23), 2010. URL http://link.aip.org/link/APPLAB/v97/i23/p234102/s1.

[87] fimecc. New coating for highly corrosive environment: Best results of the year in spinverse managed demapp-program. URL http://www.fimecc.com/fi/images/2/22/DEMAPP_MATEXON_uutinen_290910.pdf.

[88] Karen McNulty Walsh and Peter Genzer. Scientists patent corrosion-resistant nano-coating for metals. Online, May 2009. URL http://www.bnl.gov/bnlweb/pubaf/pr/PR_display.asp?prID=929.

[89] N Tsuji. Ultrafine grained steels managing both high strength and ductility. *Journal of Physics: Conference Series*, 165(1):012010, 2009. URL http://stacks.iop.org/1742-6596/165/i=1/a=012010.

[90] M. Eskandari, A. Kermanpur, and A. Najafizadeh. Formation of nano-grained structure in a 301 stainless steel using a repetitive thermo-mechanical treatment. *Materials Letters*, 63(16):1442 – 1444, 2009. URL http://dx.doi.org/10.1016/j.matlet.2009.03.043.

[91] Jr. J.W. Morris. Is there a future for nanostructured steel? In *Proceedings of the Seventeenth (2007) International Offshore and Polar Engineering Conference*, 2007.

[92] Laurence Cuffe, J.M. Don MacElroy, Matthias Tacke, Mykola Kozachok, and Damian A. Mooney. The development of nanoporous membranes for separation of carbon dioxide at high temperatures. *Journal of Membrane Science*, 272(1-2):6 – 10, 2006. URL http://dx.doi.org/10.1016/j.memsci.2005.12.021.

[93] Mario Pagliaro, editor. *Nano-Age: How Nanotechnology Changes Our Future*. Wiley-VGH, 2010.

[94] National Energy Technology Laboratory. Potential nanotechnology applications for reducing freshwater consumption at coal-fired power plants: An early view. Technical report, National Energy Technology Laboratory, 2010.

[95] Jeff Hare, George Ford, Stephanie Black, Bing Zhou, and Stan Harding. Reduction of NO_x via coal combustion catalysts. Technical report, Headwaters Incorporated, 2004. URL www.osti.gov/bridge/servlets/purl/826191-DEVox8/native/.

[96] Tinku Baidya, A. Marimuthu, M. S. Hegde, N. Ravishankar, and Giridhar Madras. Higher catalytic activity of nano-$Ce_{1-x-y}Ti_xPd_yO_{2-\delta}$ compared to nano-$Ce_{1-x}Pd_xO_{2-\delta}$ for CO oxidation and N_2O and NO reduction by CO: Role of oxide ion vacancy. *The Journal of Physical Chemistry C*, 111 (2):830–839, 2007. URL http://dx.doi.org/10.1021/jp064565e.

[97] Sounak Roy, A. Marimuthu, M.S. Hegde, and Giridhar Madras. High rates of no and n2o reduction by co, co and hydrocarbon oxidation by o2 over nano crystalline ce0.98pd0.02o2-[delta]: Catalytic and kinetic studies. *Applied Catalysis B: Environmental*, 71(1-2):23 – 31, 2007. URL http://dx.doi.org/10.1016/j.apcatb.2006.08.005.

[98] Francis J. DiSalvo. Thermoelectric Cooling and Power Generation. *Science*, 285(5428):703–706, 1999. URL http://dx.doi.org/10.1126/science.285.5428.703.

[99] David Rowe. Thermoelectric waste heat recovery as a renewable energy source. *International Journal of Innovations in Energy Systems and Power*, 1, 2006. URL www.ijesp.com/Vol1No1/IJESP1-3Rowe.pdf.

[100] T. Harman, M. Walsh, B. laforge, and G. Turner. Nanostructured thermoelectric materials. *Journal of Electronic Materials*, 34:L19–L22, 2005. URL http://dx.doi.org/10.1007/s11664-005-0083-8. 10.1007/s11664-005-0083-8.

[101] Allon I. Hochbaum, Renkun Chen, Raul Diaz Delgado, Wenjie Liang, Erik C. Garnett, Mark Najarian, Arun Majumdar, and Peidong Yang. Enhanced thermoelectric performance of rough silicon nanowires. *Nature*, 451:163–167, 2008. URL http://dx.doi.org/10.1038/nature06381.

[102] M. S. Dresselhaus, G. Chen, M. Y. Tang, R. G. Yang, H. Lee, D. Z. Wang, Z. F. Ren, J.-P. Fleurial, and P. Gogna. New directions for low-dimensional thermoelectric materials. *Advanced Materials*, 19(8):1043–1053, 2007. URL http://dx.doi.org/10.1002/adma.200600527.

[103] BioLite. Biolite, 2009. URL http://www.biolitestove.com/BioLite.html.

[104] D. Champier, J.P. Bedecarrats, M. Rivaletto, and F. Strub. Thermoelectric power generation from biomass cook stoves. *Energy*, 35(2):935 – 942, 2010. URL http://dx.doi.org/10.1016/j.energy.2009.07.015. ECOS 2008, 21st International Conference, on Efficiency, Cost, Optimization, Simulation and Environmental Impact of Energy Systems.

[105] Rida Y. Nuwayhid, Alan Shihadeh, and Nesreen Ghaddar. Development and testing of a domestic woodstove thermoelectric generator with natural convection cooling. *Energy Conversion and Management*, 46(9-10):1631 – 1643, 2005. URL http://dx.doi.org/10.1016/j.enconman.2004.07.006.

[106] Toshinori Ota, Kouichi Fujita, Susumu Tokura, and Kazuo Uematsu. Development of thermoelectric power generation system for industrial furnaces. In *Thermoelectrics, 2006. ICT '06. 25th International Conference on*, pages 354 –357, 2006. URL http://dx.doi.org/10.1109/ICT.2006.331253.

[107] Takenobu Kajikawa. Approach to the practical use of thermoelectric power generation. *Journal of Electronic Materials*, 38:1083–1088, 2009. URL http://dx.doi.org/10.1007/s11664-009-0831-2.

[108] T. Kajikawa, M. Ozaki, K. Yamaguchi, and H. Obara. Progress of development for advanced thermoelectric conversion systems. In *Thermoelectrics, 2005. ICT 2005. 24th International Conference on*, pages 162 – 169, 2005. URL http://dx.doi.org/10.1109/ICT.2005.1519910.

[109] T. Kajikawa and T. Onishi. Development for advanced thermoelectric conversion systems. In *Thermoelectrics, 2007. ICT 2007. 26th International Conference on*, pages 322 –330, 2007. URL http://dx.doi.org/10.1109/ICT.2007.4569488.

[110] Custom Thermoelectric. Power generation modules : Customthermoelectric.com. ONLINE, 2010. URL http://www.customthermoelectric.com/powergen.html.

[111] Nextreme Thermal Solutions. Thin film thermoelectric power generation. ONLINE, 2007. URL http://www.nextreme.com/media/pdf/whitepapers/Nextreme_Thin_Film.pdfl.

[112] R. Venkatasubramanian, C. Watkins, D. Stokes, J. Posthill, and C. Caylor. Energy harvesting for electronics with thermoelectric devices using nanoscale materials. In *Electron Devices Meeting, 2007. IEDM 2007. IEEE International*, pages 367 –370, dec. 2007. URL http://dx.doi.org/10.1109/IEDM.2007.4418948.

[113] Gehong Zeng, Je-Hyeong Bahk, John E. Bowers, Joshua M. O. Zide, Arthur C. Gossard, Zhixi Bian, Rajeev Singh, Ali Shakouri, Woochul Kim, Suzanne L. Singer, and Arun Majumdar. Eras:(ingaas)1-x(inalas)x alloy power generator modules. *Applied Physics Letters*, 91(26):263510 –263510–3, dec 2007. ISSN 0003-6951. URL http://dx.doi.org/10.1063/1.2828042.

[114] Timothy J. Coutts. An overview of thermophotovoltaic generation of electricity. *Solar Energy Materials and Solar Cells*, 66(1-4):443 – 452, 2001. URL http://dx.doi.org/10.1016/S0927-0248(00)00206-3.

[115] W. Durisch, B. Grob, J.-C. Mayor, J.-C. Panitz, and A. Rosselet. Interfacing a small thermophotovoltaic generator to the grid. In *AIP Conference Proceedings, Fourth NREL conference on thermophotovoltaic generation of electricity*, volume 460, pages 403 – 416, 1999. doi: 10.1063/1.57822.

[116] L M Fraas, J E Avery, H X Huang, and R U Martinelli. Thermophotovoltaic system configurations and spectral control. *Semiconductor Science and Technology*, 18(5):S165, 2003. URL http://stacks.iop.org/0268-1242/18/i=5/a=305.

[117] JX Crystals. Thermophotovoltaics. Online, 2007. URL http://www.jxcrystals.com/ThermoPV.htm.

[118] Imec. Strategy strategic program: Solar+. Online, 2009. URL http://www.imec.be/ScientificReport/SR2009/HTML/1213355.html.

[119] Prashant Nagpal, Sang Eon Han, Andreas Stein, and David J. Norris. Efficient low-temperature thermophotovoltaic emitters from metallic photonic crystals. *Nano Letters*, 8(10):3238–3243, 2008. doi: 10.1021/nl801571z. URL http://dx.doi.org/10.1021/nl801571z. PMID: 18781817.

[120] L. Bhusal and A. Freundlich. Superlattice material for the multi-junction thermophotovoltaics lattice matched to InP. In *Photovoltaic Energy Conversion, Conference Record of the 2006 IEEE 4th World Conference on*, volume 1, pages 683 –685, May 2006. URL http://dx.doi.org/10.1109/WCPEC.2006.279547.

[121] K. R. Catchpole, K. L. Lin, M. A. Green, A. G. Aberle, R. Corkish, J. Zhao, and A. Wang. Thin semiconducting layers and nanostructures as active and passive emitters for thermophotonics and thermophotovoltaics. *Physica E: Low-dimensional Systems and Nanostructures*, 14(1-2):91 – 95, 2002. URL http://dx.doi.org/10.1016/S1386-9477(02)00363-6.

[122] V.D. Rumyantsev, V.P.Khvostikov, O.A.Khvostikova, E.V.Oliva, and M.Z.Shvarts. Improvement of GaSb based TPV cells by nano-etching of diffused emitter. In *5th ISTC SAC Seminar: Nanotechnologies in the area of physics, chemistry and biotechnology*, pages 392–395, 2002.

[123] K. Qiu and A.C.S. Hayden. Thermophotovoltaic power generation systems using natural gas-fired radiant burners. *Solar Energy Materials and Solar Cells*, 91(7):588 – 596, 2007. URL http://dx.doi.org/10.1016/j.solmat.2006.11.011.

[124] L M Fraas, J E Avery, and H X Huang. Thermophotovoltaic furnace–generator for the home using low bandgap GaSb cells. *Semiconductor Science and Technology*, 18(5):S247, 2003. URL http://stacks.iop.org/0268-1242/18/i=5/a=316.

[125] Wilhelm Durisch, Bernd Bitnar, Fritz von Roth, and Günther Palfinger. Small thermophotovoltaic prototype systems. *Solar Energy*, 75(1):11 – 15, 2003. URL http://dx.doi.org/10.1016/S0038-092X(03)00232-9.

[126] L. Broman and J. Marks. Development of a tpv converter for co-generation of electricity and heat from combustion of wood powder. In *Photovoltaic Energy Conversion, 1994., Conference Record of the Twenty Fourth. IEEE Photovoltaic Specialists Conference - 1994, 1994 IEEE First World Conference on*, volume 2, pages 1764 –1766 vol.2, December 1994. URL http://dx.doi.org/10.1109/WCPEC.1994.520560.

[127] Injeti Gurrappa and Leo Binder. Electrodeposition of nanostructured coatings and their characterization—a review. *Science and Technology of Advanced Materials*, 9(4):043001, 2008. URL http://stacks.iop.org/1468-6996/9/i=4/a=043001.

[128] Jong-Hee Park and T. S. Sudarshan. *Chemical Vapor Deposition*. ASM International, 2003.

[129] Chue San Yoo. *Semiconductor Manufacturing Technology*. World Scientific Publishing Co. Pted. Ltd., 2008.

[130] Evelyn Schmich, Norbert Schillinger, and Stefan Reber. Silicon cvd deposition for low cost applications in photovoltaics. *Surface and Coatings Technology*, 201(22-23):9325 – 9329, 2007. URL http://dx.doi.org/10.1016/j.surfcoat.2007.04.089. Euro CVD 16, 16th European Conference on Chemical Vapor Deposition.

[131] Dunwei Wang and Hongjie Dai. Low-temperature synthesis of single-crystal germanium nanowires by chemical vapor deposition. *Angewandte Chemie*, 114(24):4977–4980, 2002. URL http://dx.doi.org/10.1002/ange.200290046.

[132] Jae-Ryoung Kim, Hye Mi So, Jong Wan Park, Ju-Jin Kim, Jinhee Kim, Cheol Jin Lee, and Seung Chul Lyu. Electrical transport properties of individual gallium nitride nanowires synthesized by chemical-vapor-deposition. *Applied Physics Letters*, 80, 2002. URL http://dx.doi.org/10.1063/1.1478158.

[133] T. I. Kamins, R. Stanley Williams, D. P. Basile, T. Hesjedal, and J. S. Harris. Ti-catalyzed si nanowires by chemical vapor deposition: Microscopy and growth mechanisms. *Journal of Applied Physics*, 89, 2001. URL http://dx.doi.org/10.1063/1.1335640.

[134] Jürgen M. Lackner. Industrially-scaled large-area and high-rate tribological coating by pulsed laser deposition. *Surface and Coatings Technology*, 200(5-6):1439 – 1444, 2005. URL http://dx.doi.org/10.1016/j.surfcoat.2005.08.029. ICMCTF 2005.

[135] Guozhong Cao. *Nanostructures & Nanomaterials: synthesis, properties & applications*. Imperial College Press.

[136] Richter Precision Inc. PVD coatings - physical vapor deposition. Online, 2010. URL http://www.richterprecision.com/pvd-coatings.html.

[137] Applied Materials. Akt pivot pvd system for tft-lcd array. Online, 2010. URL http://www.appliedmaterials.com/technologies/library/akt-pivot-pvd-system-tft-lcd-array.

[138] Mohamed Henini. Molecular beam epitaxy from research to mass-production – part ii. *III-Vs Review*, 9(4):33 – 36, 1996. URL http://dx.doi.org/10.1016/S0961-1290(96)80234-1.

[139] Mikko Ritala and Markku Leskelä. *Handbook of Thin Film Materials, Volume 1: Deposition and Processing of Thin Films*, chapter Atomic Layer Deposition. 2002.

[140] Rachel A. Caruso and Markus Antonietti. Sol-gel nanocoating: An approach to the preparation of structured materials. *Chemistry of Materials*, 13(10):3272–3282, 2001. URL http://dx.doi.org/10.1021/cm001257z.

[141] Alain C. Pierre. *Introduction to Sol-Gel Processing*. Kluwer Academic Publisher, 1998.

[142] John D. Wright and Nico A.J.M. Sommerdijk. *Sol-Gel Materials: Chemistry and Applications*. CRC Press, 2000.

[143] A.A. Youssef, P. Budzynski, J. Filiks, A.P. Kobzev, and J. Sielanko. Improvement of wear and hardness of steel by nitrogen implantation. *Vacuum*, 77(1):37 – 45, 2004. URL http://dx.doi.org/10.1016/j.vacuum.2004.07.069.

[144] S. Lo Russo, P. Mazzoldi, I. Scotoni, C. Tosello, and S. Tosto. Effect of nitrogen-ion implantation on the unlubricated sliding wear of steel. *Applied Physics Letters*, 34(10):627 –629, May 1979. URL http://dx.doi.org/10.1063/1.90641.

[145] M.E. Chabica, D.L. Williamson, R. Wei, and P.J. Wilbur. Microstructure and corrosion of nitrogen implanted AISI 304 stainless steel. *Surface and Coatings Technology*, 51(1-3):24 – 29, 1992. URL http://dx.doi.org/10.1016/0257-8972(92)90209-S.

[146] Gianluca Cassaro Yuchun Xu, Rajkumar Roy and Jeremy Ramsden. *Development of a Cost Estimating Framework for Nanotechnology Based Products*. 2009. URL http://dx.doi.org/10.1007/978-1-84882-762-2_18.

[147] Y.T. Pei, D. Galvan, J.Th.M. De Hosson, and A. Cavaleiro. Nanostructured TiC/a-C coatings for low friction and wear resistant applications. *Surface and Coatings Technology*, 198(1-3):44 – 50, 2005. URL http://dx.doi.org/10.1016/j.surfcoat.2004.10.106.

[148] Petr Vasina, Pavel Soucek, Tereza Schmidtová, Marek Eliás, Vilma Bursíková, Mojmír Jílek, Mojmír Jílek Jr., Jan Schäfer, and Jirí Bursík. Depth profile analyses of nc-TiC/a-C:H coating prepared by balanced magnetron sputtering. *Surface and Coatings Technology*, In Press, Corrected Proof:–, 2011. URL http://dx.doi.org/10.1016/j.surfcoat.2011.02.038.

[149] Kurt J. Lesker Company. Deposition sources. Online, 2011. URL http://www.lesker.com/newweb/menu_depositSources.cfm.

[150] Hyung-Jun Kim, Chang-Hee Lee, and Soon-Young Hwang. Superhard nano wc-12% co coating by cold spray deposition. *Materials Science and Engineering A*, 391(1-2):243 – 248, 2005. URL http://dx.doi.org/10.1016/j.msea.2004.08.082.

[151] B. Kear, R. Sadangi, M. Jain, R. Yao, Z. Kalman, G. Skandan, and W. Mayo. Thermal sprayed nanostructured WC/Co hardcoatings. *Journal of Thermal Spray Technology*, 9:399–406, 2000. URL http://dx.doi.org/10.1361/105996300770349863. 10.1361/105996300770349863.

[152] Z. Ban and L. Shaw. Characterization of thermal sprayed nanostructured WC-Co coatings derived from nanocrystalline WC-18wt.%Co powders. *Journal of Thermal Spray Technology*, 12:112–119, 2003. URL http://dx.doi.org/10.1361/105996303770348564. 10.1361/105996303770348564.

[153] Roland Streiff, John Stringer, Richard Krutenat, Marcel Caillet, and Robert Rapp. An assessment of thermal spray coating technologies for high temperature corrosion protection. *Materials Science Forum*, 251 - 254:809–816, 1997. URL www.castolin.com/wCastolin_com/pdf/publications/essai7.pdf.

[154] CiperTech. Cipertech wc-co spray powder. ONLINE, 2011. URL http://cipertech.com/html_products/WC-Co-Spray-Powder-27.html.

[155] M.D. Rowe, Gao Min, S.G.K. Williams, A. Aoune, K. Matsuura, V.L. Kuznetsov, and Li Wen Fu. Thermoelectric recovery of waste heat-case studies. In *Energy Conversion Engineering Conference, 1997. IECEC-97., Proceedings of the 32nd Intersociety*, pages 1075 –1079 vol.2, jul-1 aug 1997. URL http://dx.doi.org/10.1109/IECEC.1997.661919.

[156] Bed Poudel, Qing Hao, Yi Ma, Yucheng Lan, Austin Minnich, Bo Yu, Xiao Yan, Dezhi Wang, Andrew Muto, Daryoosh Vashaee, Xiaoyuan Chen, Junming Liu, Mildred S. Dresselhaus, Gang Chen, and Zhifeng Ren. High-thermoelectric performance of nanostructured bismuth antimony telluride bulk alloys. *Science*, 320(5876):634–638, 2008. URL http://dx.doi.org/10.1126/science.1156446.

[157] Shufen Fan, Junnan Zhao, Jun Guo, Qingyu Yan, Jan Ma, and Huey Hoon Hng. p-type Bi[sub 0.4]Sb[sub 1.6]Te[sub 3] nanocomposites with enhanced figure of merit. *Applied Physics Letters*, 96 (18):182104, 2010. URL http://dx.doi.org/10.1063/1.3427427.

[158] Economic analysis in the optimization of belt conveyor systems.

[159] Inframat Advanced Materials LLC. Inframat advanced materials. Online, 2010. URL http://www.advancedmaterials.us/.

[160] Gary Heath and John Skora. New materials & process developments for perventative maintenance and repair in cement plants. In *40th Cement Industry Technical Conference XL Conference Record*, 1998. URL http://www.castolin.com/wCastolin_com/pdf/publications/essai3_part1.pdf.

[161] Gerhardus Koch. Cost of corrosion: Electrical utilities. Technical report, CC Technologies Laboratories, 2001.

[162] Energiateollisuus. Electricity year 2010, 2011. URL http://www.energia.fi/en/news/electricity%20year%202010.html.

[163] D.M. Rowe, editor. *CRC Handbook of Thermoelectrics*. CRC-Press, 1995.

[164] A. Markoliya, N. Sudak, E. Sabo, S. Krivoruchko, T. Vekua, N. Grechko, Yu. Dudarev, M. Maksimov, A. Surovtseva, A. Chilikidi, V. Shamba, R. Shvangiradze, and Yu. Éloshvili. Development and improvement of thermoelectric generator modules for a space nuclear power system. *Atomic Energy*, 89:583–586, 2000. URL http://dx.doi.org/10.1007/BF02673519.

[165] NASA. Voyager weekly reports. ONLINE, 2011. URL http://voyager.jpl.nasa.gov/mission/weekly-reports/.

[166] P.J. Owen and P.W. Cleary. Prediction of screw conveyor performance using the discrete element method (DEM). *Powder Technology*, 193(3):274 – 288, 2009. URL http://dx.doi.org/10.1016/j.powtec.2009.03.012. Special Issue: Discrete Element Methods: The 4th International conference on Discrete Element Methods, The 4th International Conference on Discrete Element Methods, Brisbane, August 2007.

[167] P.J. Owen and P.W. Cleary. Screw conveyor performance: comparison of discrete element modelling with laboratory experiments. In *Seventh International Conference on CFD in the Minerals and Process Industries*, December 2009. URL www.cfd.com.au/cfd_conf09/PDFs/132OWE.pdf.

[168] Ralf Riedel, editor. *The Handbook of Ceramic Hard Materials*. Wiley-VCH, 2000.

[169] Rob Ramsdale. The engineers handbook, 2006. URL http://www.engineershandbook.com.